AD NUMBER

ADB006667

LIMITATION CHANGES

TO:

Approved for public release; distribution is unlimited.

FROM:

Distribution authorized to U.S. Gov't. agencies only; Test and Evaluation; 28 MAY 1975. Other requests shall be referred to Air Force Cambridge Research Labs., Hanscom AFB, MA.

AUTHORITY

AFCRL ltr 1 Aug 1983

Ficha 1

AD B006667

AUTHORITY: USAFGL
ltr, 1 Aug 83

AFCRL-TR-75-0302
AIR FORCE SURVEYS IN GEOPHYSICS, NO. 320

Final Report of PVM-5 Weather Documentation AFCRL/Minuteman Report No. 4

JAMES I. METCALF, Capt, USAF
ARNOLD A. BARNES, Jr.
MICHAEL J. KRAUS

28 May 1975

METEOROLOGY LABORATORY PROJECT 133B
AIR FORCE CAMBRIDGE RESEARCH LABORATORIES
HANSCOM AFB, MASSACHUSETTS 01731

AIR FORCE SYSTEMS COMMAND, USAF

Unclassified

SECURITY CLASSIFICATION OF THIS PAGE (When Data Entered)

REPORT DOCUMENTATION PAGE		READ INSTRUCTIONS BEFORE COMPLETING FORM
1. REPORT NUMBER AFCRL-TR-75-0302	2. GOVT ACCESSION NO.	3. RECIPIENT'S CATALOG NUMBER
4. TITLE (and Subtitle) FINAL REPORT OF PVM-5 WEATHER DOCUMENTATION AFCRL/MINUTEMAN REPORT NO. 4		5. TYPE OF REPORT & PERIOD COVERED Scientific. Final. 6. PERFORMING ORG. REPORT NUMBER AFSG, No. 320
7. AUTHOR(s) James I. Metcalf, Capt, USAF Arnold A. Barnes, Jr. Michael J. Kraus		8. CONTRACT OR GRANT NUMBER(s)
9. PERFORMING ORGANIZATION NAME AND ADDRESS Meteorology Laboratory (LY) Air Force Cambridge Research Laboratories Hanscom AFB, Mass. 01731		10. PROGRAM ELEMENT, PROJECT, TASK AREA & WORK UNIT NUMBERS 133B0001
11. CONTROLLING OFFICE NAME AND ADDRESS Meteorology Laboratory (LYW) Air Force Cambridge Research Laboratories Hanscom AFB, Mass. 01731		12. REPORT DATE 28 May 1975 13. NUMBER OF PAGES
14. MONITORING AGENCY NAME & ADDRESS(if different from Controlling Office)		15. SECURITY CLASS. (of this report) Unclassified 15a. DECLASSIFICATION/DOWNGRADING SCHEDULE

16. DISTRIBUTION STATEMENT (of this Report)

Distribution limited to U.S. Government agencies only; (Test and Evaluation; Test & Evaluation of Military Systems/Equipment); (28 May 1975). Other requests for this document must be referred to AFCRL/LYW, Hanscom AFB, Massachusetts 01731.

17. DISTRIBUTION STATEMENT (of the abstract entered in Block 20, if different from Report)

18. SUPPLEMENTARY NOTES

TECH. OTHER.

19. KEY WORDS (Continue on reverse side if necessary and identify by block number)

Minuteman
Aircraft weather measurement
Radar weather measurement
Tropical cirrus cloud
Water content profiles

20. ABSTRACT (Continue on reverse side if necessary and identify by block number)

Reentry weather encountered by Minuteman test PVM-5 is described. Documentation was accomplished by WB-57F aircraft, by satellite, by radar, and by lidar. All RV's passed through a cloud layer with maximum ice water content of 0.03 to 0.08 gm m^{-3}. Weather Severity Indices were 0.8, 0.6, and 0.3 for RV1, 2, and 3. Precise definition of the reentry weather was made possible by correlation of simultaneous weather measurements by aircraft and radar after the reentry. These measurements were performed by means of the

DD FORM 1 JAN 73 1473 EDITION OF 1 NOV 65 IS OBSOLETE

Unclassified

SECURITY CLASSIFICATION OF THIS PAGE (When Data Entered)

link-offset mode, in which the radar weather data were recorded at a fixed distance ahead of the aircraft.

Preface

The development of the Minuteman Natural Hazards Program and AFCRL participation in the program have been described in previous reports in this series. The PVM-5 test was the first in which the reentry vehicles were intentionally flown through clouds, and quantitative documentation of the weather was therefore essential. The data acquisition plan incorporated several improvements over previous operations. In particular, the link-offset mode was used to obtain correlation weather data from the aircraft and radar. Use of radar cross-section data recorded in real time at the PRESS computer permitted the calculation of reflectivity profiles on the trajectories for short-term pre-mission forecasting and greatly facilitated the entire weather data analysis. The analysis of the correlation data was described in detail in the first report in this series (see list below) and is summarized in Section 4.

The field support included representatives of SAMSO/MN; AFCRL Meteorology Laboratory; SAMTEC/WE; 9th Weather Reconnaissance Wing (58th Weather Reconnaissance Squadron); 6th Weather Wing; TRW Systems Group; Meteorology Research, Inc.; Science Applications, Inc.; Edgerton, Germeshausen, and Grier, Inc.; Particle Measuring Systems, Inc.; and Stanford Research Institute. TRW was responsible for the overall planning and operation of the test.[1] The roles of the other organizations are described in our report. In particular, MRI

---

1. Wilmot, R.A., Cisneros, C.E., and Guiberson, F.L. (1974) High cloud measurements applicable to ballistic missile systems testing, 6th Conf. Aerosp. and Aeronaut. Meteor., Amer. Meteor. Soc., 194-199.

was responsible for the operation of the aircraft instrumentation[2] (except the holographic camera), and the lidar[3] was operated by SRI. Readers interested in more details of their equipment or data than are presented here are referred to their final reports.

Reports prepared to date in the AFCRL/Minuteman Series are as follows:

1. "Aircraft and Radar Weather Data Analysis for PVM-5"[4] is a description of the link-offset mode of radar and aircraft operations. We provide examples of the data obtained and application of the correlation results to obtain definition of the ice water content along the reentry trajectories.

2. "Final Report of PVM-4 and PVM-3 Weather Documentation"[5] is a summary of the weather observed by the available sensors operating during these missions.

3. "Final Report of STM-8W Weather Documentation"[6] is a summary of the weather during this clear-air mission and a description of the initial test of the link-offset mode using the TTR-4 radar and one of the WB-57F aircraft.

Two additional papers have been prepared under this project for presentation at professional conferences.[7, 8]

---

2. Jahnsen, L.J., Heymsfield, A.J., and Carbone, R.E. (1974) Final Report of PVM-5 Mission and NEWT WB-57F Instrumentation and Cloud Particle Measurements, MRI 74 FR-1230, Meteorology Research, Inc., Altadena, Calif.

3. Uthe, E.E., Allen, R.J., and Russell, P.B. (1974) Light Detection and Ranging (LIDAR) Support for STM-8W and PVM-5 Reentry Operations, SRI Project 2859, Stanford Research Institute, Menlo Park, Calif.

4. Barnes, A.A., Jr., Metcalf, J.I., and Nelson, L.D. (1974) Aircraft and Radar Weather Data Analysis for PVM-5, AFCRL-TR-74-0627, Air Force Cambridge Research Laboratories, Hanscom AFB, Mass.

5. Metcalf, J.I., Barnes, A.A., Jr., and Kraus, M.J. (1975) Final Report of PVM-4 and PVM-3 Weather Documentation, AFCRL-TR-75-0097, Air Force Cambridge Research Laboratories, Hanscom AFB, Mass.

6. Metcalf, J.I., Barnes, A.A., Jr., and Kraus, M.J. (1975) Final Report of STM-8W Weather Documentation, AFCRL-TR-75-0207, Air Force Cambridge Research Laboratories, Hanscom AFB, Mass.

7. Barnes, A.A., Jr., Nelson, L.D., and Metcalf, J.I. (1974) Weather documentation at Kwajalein Missile Range, 6th Conf. Aerosp. and Aeronaut. Meteor., Amer. Meteor. Soc., pp 66-69; AFCRL-TR-74-0430, Air Force Cambridge Research Laboratories, Hanscom AFB, Mass.

8. Metcalf, J.I., Barnes, A.A., Jr., and Nelson, L.D. (1975) Water content and reflectivity measurement by "chirp" radar, 16th Radar Meteor. Conf., Amer. Meteor. Soc., pp 492-495.

Contents

1.	INTRODUCTION	7
2.	WEATHER DESCRIPTION	9
3.	WB-57F WEATHER OBSERVATIONS	17
4.	ALCOR WEATHER OBSERVATIONS	24
5.	SUMMARY AND CONCLUSIONS	38
REFERENCES		41
APPENDIX A.	Derivation and Processing of PRESS B-6 Data	43
ACRYONYMS AND SYMBOLS		45

Illustrations

1.	Kwajalein Atoll, Showing the Islands Occupied by the Facilities of Kwajalein Missile Range	8
2.	DMSP Satellite Visual Data for 4 April 1974, 2331Z	10
3.	Montage of Photographs from WB-57F Downward-Looking Camera	11
4.	Sounding from (a) Kwajalein at 0153Z, 5 April 1974, and (b) Roi-Namur at 0154Z, 5 April 1974	13

Illustrations

5. Cloud Echoes Recorded by TPQ-11 Vertically Pointing Radar at Kwajalein, 1320 to 1440Z, 5 April 1974 14
6. WSR-57 Radar PPI at 0153Z, 5 April 1974 14
7. Height-Time Display from the SRI Mark IX Lidar at Gellinam, 0030 to 0220Z, 5 April 1974 (1230 to 1420 local time, 4 April 1974) 16
8. Instrumentation Pod on Right Wing of WB-57F Aircraft 20
9. Instrumentation Pod on Left Wing of WB-57F Aircraft 20
10. Flight Tracks for Correlation Operations and PVM-5 Reentry Trajectories 22
11. WSR-57 Radar PPI at 0310 and 0340Z, 5 April 1974 23
12. Radar Weather Data Flow Diagram 27
13. ALCOR RHI Scans During PVM-5 Operations 29
14. Profiles of Radar Reflectivity Factor Z on PVM-5 RV1 Trajectory 30
15. ALCOR Scan of PVM-5 RV1 Trajectory at 0156Z, 5 April 1974 31
16. Profiles of Radar Reflectivity Factor Z on PVM-5 RV2 Trajectory 32
17. ALCOR Scan of PVM-5 RV2 Trajectory at 0157Z, 5 April 1974 33
18. Profiles of Radar Reflectivity Factor Z on PVM-5 RV3 Trajectory 34
19. ALCOR Scan of PVM-5 RV3 Trajectory at 0155Z, 5 April 1974 35
20. Profiles of Reflectivity Factor Z on ALCOR Vertical Scans at 0158 to 0207Z, 5 April 1974 37
21. Composite of Z-M Equations Derived from PVM-5 Aircraft and Radar Weather Data 38
22. Profiles of Ice Water Content on the PVM-5 Trajectories 39
23. Variations of WSI During the PVM-5 Trajectory Weather Scans 39

Tables

1. Lidar Data Summary, March-April 1974 15
2. WB-57F Operations at Kwajalein, March-April 1974 18
3. ALCOR/PRESS Weather Support, March-April 1974 25

Final Report of PVM-5 Weather Documentation AFCRL/Minuteman Report No. 4

1. INTRODUCTION

The Minuteman PVM-5 test was launched on 5 April 1974, with reentry near Kwajalein Atoll at 0153Z. This report describes the weather data acquisition plan and presents our final determination of the water content profiles encountered by the reentry vehicles. Data from various meteorological sensors are presented to provide further details on the local weather, both on the macroscale of clouds and weather systems and on the microscale of particle shapes and sizes.

Descriptions of each of the sensors are included with the presentations of data in the following sections. The locations of the various supporting facilities are shown in Figure 1. The NWS operated a rawinsonde site at Roi-Namur in addition to rawinsonde and weather radar facilities on Kwajalein Island. The DMSP satellite van operated by personnel from the 6th Weather Wing, McClellan AFB, was located on Kwajalein Island. The lidar operated by SRI was located on Gellinam Island, close to the reentry corridor. The Lincoln Laboratory radars, located at KREMS on Roi-Namur Island, were used to obtain weather data on the reentry trajectories. Two WB-57F aircraft operated by the 58th Weather Reconnaissance Squadron from Kirtland AFB were based at Kwajalein for the PVM-5 test support.

Execution of the weather data acquisition plan and on-site evaluation of the data were the responsibilities of the mission Weather Team, which was at

(Received for publication 28 May 1975)

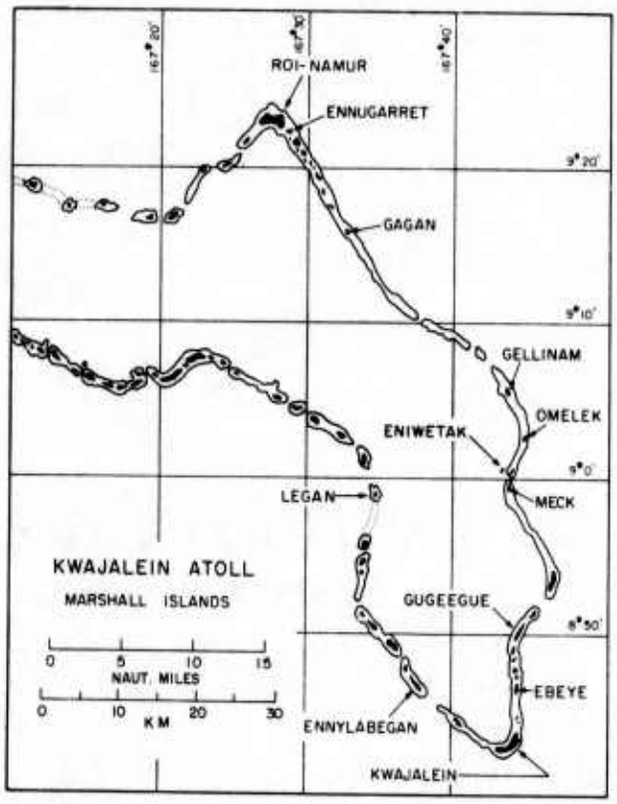

Figure 1. Kwajalein Atoll, Showing the Islands Occupied by the Facilities of Kwajalein Missile Range. Range Operations Control Center, aircraft support facilities, NWS radars, and MPS-36 radars are at Kwajalein Island. Lincoln Laboratory radars are at Roi-Namur Island

Kwajalein during the period 21 March to 6 April 1974. The Weather Team included representatives of AFCRL,* SAMSO, SAMTEC, TRW, and MRI at the ROCC and two AFCRL meteorologists** at KREMS.

The reentry weather criterion was in terms of the Weather Severity Index, defined as

$$WSI \equiv \int_{h_1}^{h_2} M\, h\, dh\,, \tag{1}$$

where h_1 is the height (km) of the lowest cloud base and h_2 is the height of the highest cloud top on the trajectory. For a series of thin layers, or for numerical integration across a thick cloud layer this may be approximated by

* L.D. Nelson.

** C.N. Touart and A.A. Barnes, Jr.

$$WSI \cong \sum_i M_i \bar{h}_i \Delta h_i \qquad (2)$$

$$\cong \sum_i M_i \frac{(h_i + h_{i-1})}{2} (h_i - h_{i-1})$$

$$= \sum_i M_i \frac{h_i^2 - h_{i-1}^2}{2} . \qquad (3)$$

The criterion for PVM-5 was WSI > 6 (Minuteman/TRW planning information received by AFCRL on 5 Feb 1974).

The RV's passed through a cloud layer, or series of layers, that was 3 to 4 km thick with maximum ice water content about 0.08 gm m^{-3} (RV2). The three RV's encountered WSI of 0.8, 0.6, and 0.3. The cloud structure in the reentry corridor was documented primarily by the WB-57F aircraft, ALCOR, and the SRI lidar. Joint measurements of reflectivity by ALCOR and ice water content by the WB-57F made possible the derivation of Z-M correlation equations for interpreting the radar weather scans along the trajectories.

2. WEATHER DESCRIPTION

The reentry weather on 5 April 1974 was related to a major upper-level trough which was developing some 550 km west of Kwajalein on 1 April. Continuing development of this trough produced significant convective activity and widespread cirrus in the vicinity of Kwajalein on 3 and 4 April. The DMSP satellite photo on 4 April at 2331Z (Figure 2) showed the cirrus extending some 125 km to the north, 300 km to the south, and 450 to 550 km to the east from Kwajalein. As on the previous day, the high-level clouds were moving from the southwest, at speeds of 5 to 15 m sec^{-1}. Close examination of the satellite photo reveals considerable variation of the cloud structure even within 50 to 100 km of Kwajalein. This small-scale variability was of great concern to the mission weather forecasters in preparing their short-term forecast and launch recommendation. Detailed examination of the cloud structure as revealed by all the weather sensors has made it possible to describe precisely the variations through the reentry corridor and the differences in the weather encountered by the three RV's.

The WB-57F aircraft sampled the clouds in the reentry corridor from 0025Z to 0135Z between 6 and 12 km. The thickest clouds had tops at 10.7 km altitude,

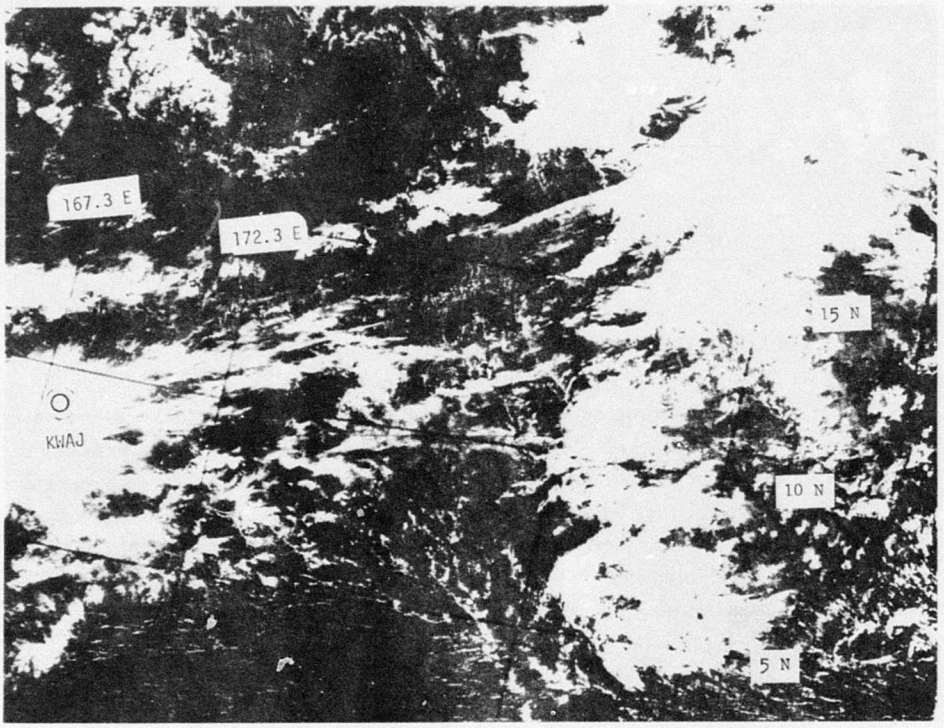

Figure 2. DMSP Satellite Visual Data for 4 April 1974, 2331Z. A major weather system to the west is producing widespread cloudiness, with the high-level cirrus moving from the southwest through the reentry corridor. Considerable convective activity is embedded in the large cloud mass

with thinner clouds above them extending to an altitude of 11.7 km. Northeast of the corridor the clouds appeared nearly continuous from the bottom of the aircraft soundings, and the cloud top appeared fairly uniform. To the southwest and west there was a distinct upper layer of broken cirrus near 11.7 km, and thick cloud below 9.5 km with some convective tops above 10 km. Highest values of ice water content were about 0.1 gm m^{-3}, observed near 7 km. Coincident with the reentry the WB-57F began a photo-mapping pass at 16 km altitude, heading north at a longitude of 167°34'E. The photographs (Figure 3) showed a relatively clear area extending into the reentry corridor from the southwest. Part of the eastern reef could be seen faintly under the edge of the thicker cloud to the east. The indistinct appearance of the low-level clouds and the islands indicated that a high thin cirrus layer covered this area. The general structure was consistent with

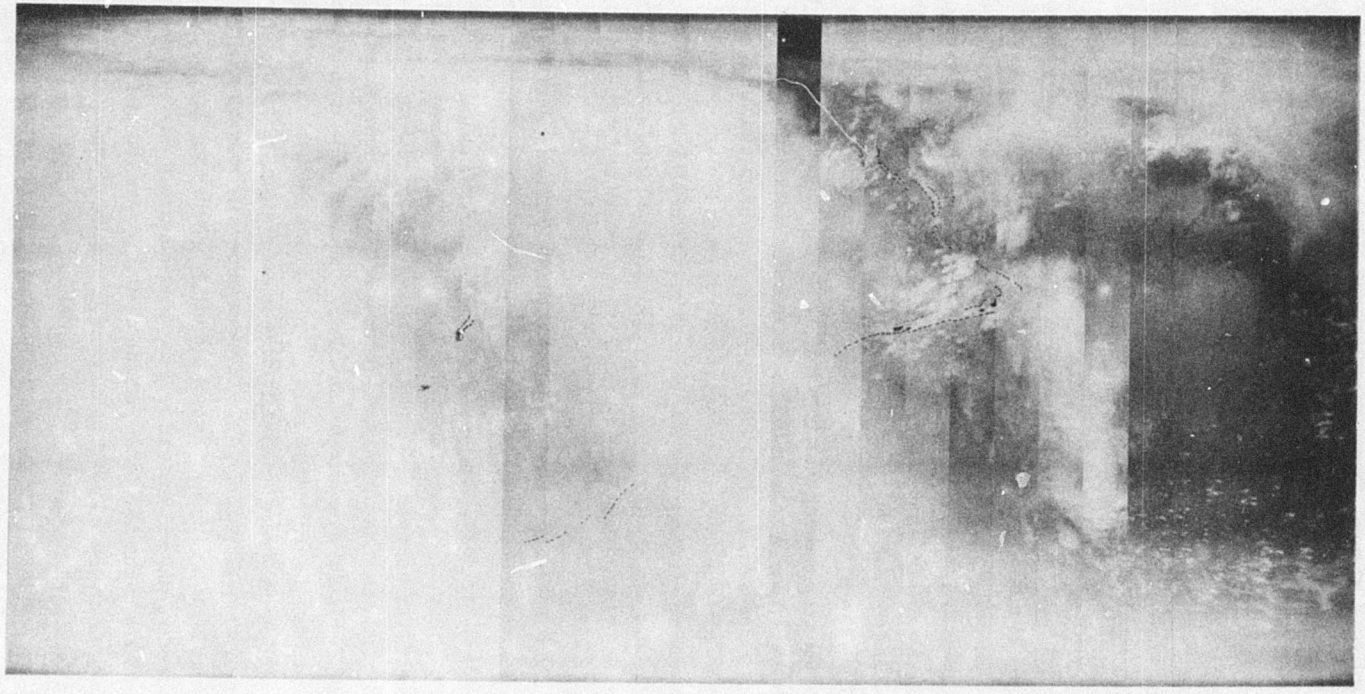

Figure 3. Montage of Photographs from WB-57F Downward-Looking Camera. Flight is at 16 km altitude on a northerly heading at a longitude of 167° 34' at 0152 to 0159Z. Islands of Eller and Ennugenliggelap (first and second north of Legan) and sun glint on the water, are seen through a break in the clouds in the left side of the panorama. Part of the northern tip of the atoll can be seen, although Roi-Namur is mostly covered by clouds. View of low-level features is not distinct, except in the right (northern) side of the panorama, indicating that a thin high-level cirrus layer covers the reentry area

the earlier aircraft observations. Recalling the upper cirrus layer observed toward the southwest, we conclude that this layer covered the reentry area, and that the relatively clear areas were due to breaks in the clouds below 10 km. To the north of the relatively clear area the thick clouds extended to within about 15 km of Roi-Namur, and a smaller, separate patch of cirrus was located just above and to the northeast of Roi-Namur. The continuity of the upper cirrus layer is indicated also by its detection on the ALCOR RV1 and vertical weather scans which are described more fully in Section 4. This layer probably extended to the other trajectories, but was too thin to be detectable by ALCOR.

The NWS soundings from Kwajalein and Roi-Namur (Figure 4) showed common features of the winds at these locations. Winds were generally from the east-southeast from the surface to 3.7 km, then strongly from the northeast at speeds up to 12 m sec^{-1} above 4.5 km. A sharp transition to southwesterly flow occurred about 7.9 km on the Kwajalein sounding and 6.7 km at Roi-Namur. The southwesterly flow extended to 12.8 km, with speeds up to 19 m sec^{-1} at 12.2 km. Between 13 and 17 km the wind veered gradually to north-northwest with decreasing speed. Just below the tropopause, which was at 17.7 km, the wind switched to southerly or southwesterly at 4 to 8 m sec^{-1}. Above the tropopause the wind was again from the west-northwest to about 20 km. Both soundings showed a moist surface layer with a relatively dry layer separating it from the more humid layer above. The relatively dry layer (RH < 50 percent) occurred at 5.2 to 5.5 km at Kwajalein and 4.9 to 6.4 km at Roi-Namur, and the observed tops of this layer coincided with the cloud bases observed by the TPQ-11 radar at Kwajalein and ALCOR at Roi-Namur.

The NWS 0.86-cm TPQ-11 radar is capable of detecting non-precipitating clouds, but is subject to strong attenuation in precipitation. It functions excellently as a ceilometer, but cannot give a reliable measurement of the vertical extent of a thick cloud layer. About the time of reentry (Figure 5) the TPQ-11 showed a fairly uniform cloud layer between 5.5 and 9.1 km, with intermittent clouds up to 11 km. This is at variance with the reports from the WB-57F crew that the thick clouds northeast of Kwajalein extended to 10.7 km, with some thin clouds above, and indicates attenuation of the TPQ-11 radar signal in the thick clouds. The 10-cm WSR-57 radar, which is only capable of detecting precipitation, showed numerous echoes in the reentry area (Figure 6). These were generally moving toward the west-northwest, that is, with the wind below 4 km. However, the larger cells were undoubtedly feeding the widespread cirrus, particularly the large precipitation area at 40 to 85 km to the northeast and the cell at 45 km and 285°, both of which were observed from the WB-57F to be penetrating the highest cloud layers.

The SRI Mark IX lidar[3] was at KMR from 25 March to 5 April 1974. The Mark IX system uses a pulsed ruby laser operating at a wavelength of 6943 Å.

(a)

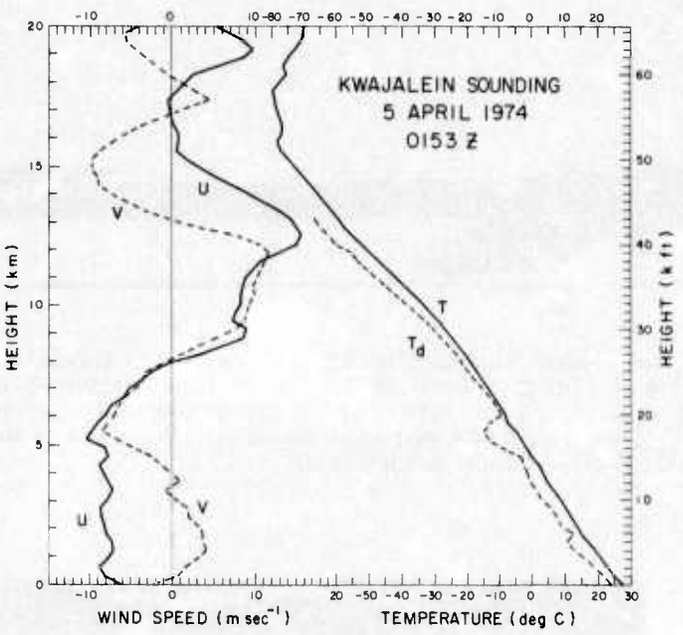

(b)

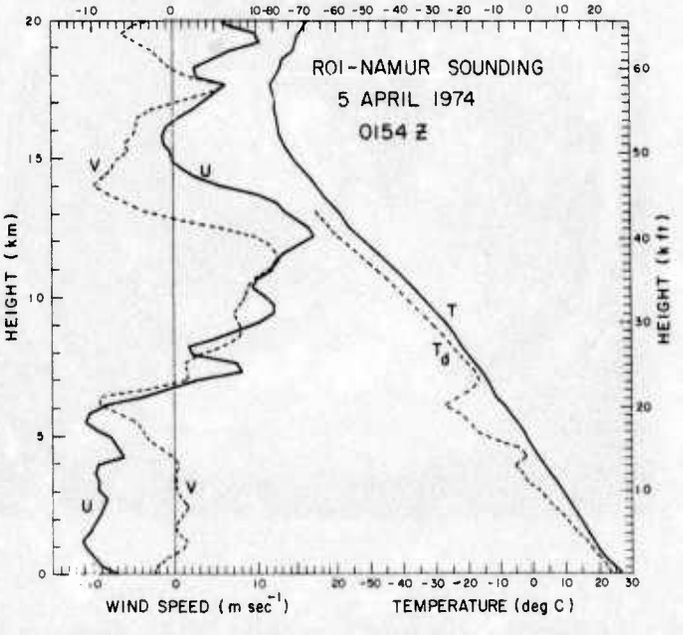

Figure 4. Sounding from (a) Kwajalein at 0153Z, 5 April 1974, and (b) Roi-Namur at 0154Z, 5 April 1974. Wind components are plotted toward the east (U) and toward the north (V). Wind structure varies sharply with height, with strong flow from the northeast, up to 12 m sec^{-1}, between 4.5 and 7.9 km, and southwesterly flow between 7.9 and 12.2 km with speeds up to 19 m sec^{-1}. A relatively dry layer (RH < 50 percent) about 5 to 6 km altitude separates the moist surface layer from the moist layer, corresponding to the cloud layer, above. Humidity values taper off gradually above 7 km, but no distinct top of the upper moist layer is evident

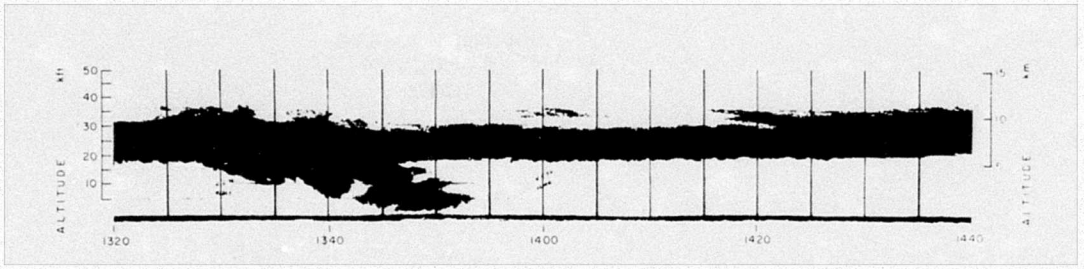

Figure 5. Cloud Echoes Recorded by TPQ-11 Vertically Pointing Radar at Kwajalein, 1320 to 1440Z, 5 April 1974. Height-time display shows very uniform base of cloud layer at 5.5 km, with one low-level cloud passing over the radar at 1340 to 1350. Irregularity of cloud structure above 9 km is due to attenuation of the 0.86-cm (34.9 GHz) signal in the clouds

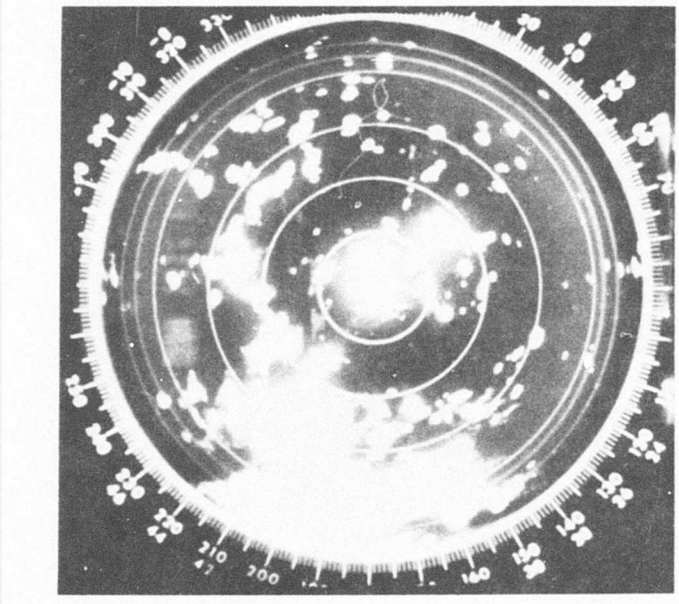

Figure 6. WSR-57 Radar PPI at 0153Z, 5 April 1974. Elevation angle is 0^{o} and range markers are at 25 nmi (46.3 km) intervals out to 125 nmi (231.5 km). Most extensive precipitation is to the south of Kwajalein, but significant showers are present to the north and northeast near the reentry corridor

Backscattered signal intensity, which depends primarily on the integrated cross-sectional area of the cloud or aerosol particles, was measured and provided a means of determining ice water content or density. Signal attenuation or multiple scattering may limit the accuracy of the lidar measurements in thick clouds or precipitation. A summary of the lidar operations is presented in Tab'e 1.

Table 1. Lidar Data Summary, March-April 1974

Date (1974)	Start-Stop (GMT)	Number of Shots	Fire Rate (pulses/ minute)	Remarks
26 March	2000-2032	160	5	
	2040-0030 (27 March)	800	4	Power failure
27 March	0110-0142	160	5	
28 March	2001-0211 (29 March)	1,837	5	Thin-dense cirrus returns
1 April	1948-2020	160	5	Extremely thin layer at 14.3 km
3 April	0155-0558	1,209	5	Dense cirrus at 9.1 km for first data runs
3 April	2005-2215	640	5	Stop for rain
	2303-0327 (4 April)	1,212	5	Good cirrus structure
				PVM-5 mission day
4 April	2045-2117	160	5	
	2130-2240	160	--	Polarization experiment
	2242-0141 (5 April)	834	5	
5 April	0144-0154	165	20	Angular scans: Azimuth = 52° Elevation = 35° to 70°
	0155-0219	480	20	Vertical
	0221-0224	80	20	Angular scans: Azimuth = 52° Elevation = 10° to 90°
	0227-0235	160	20	Vertical
	0235-0429	571	5	During aircraft/radar correlation runs

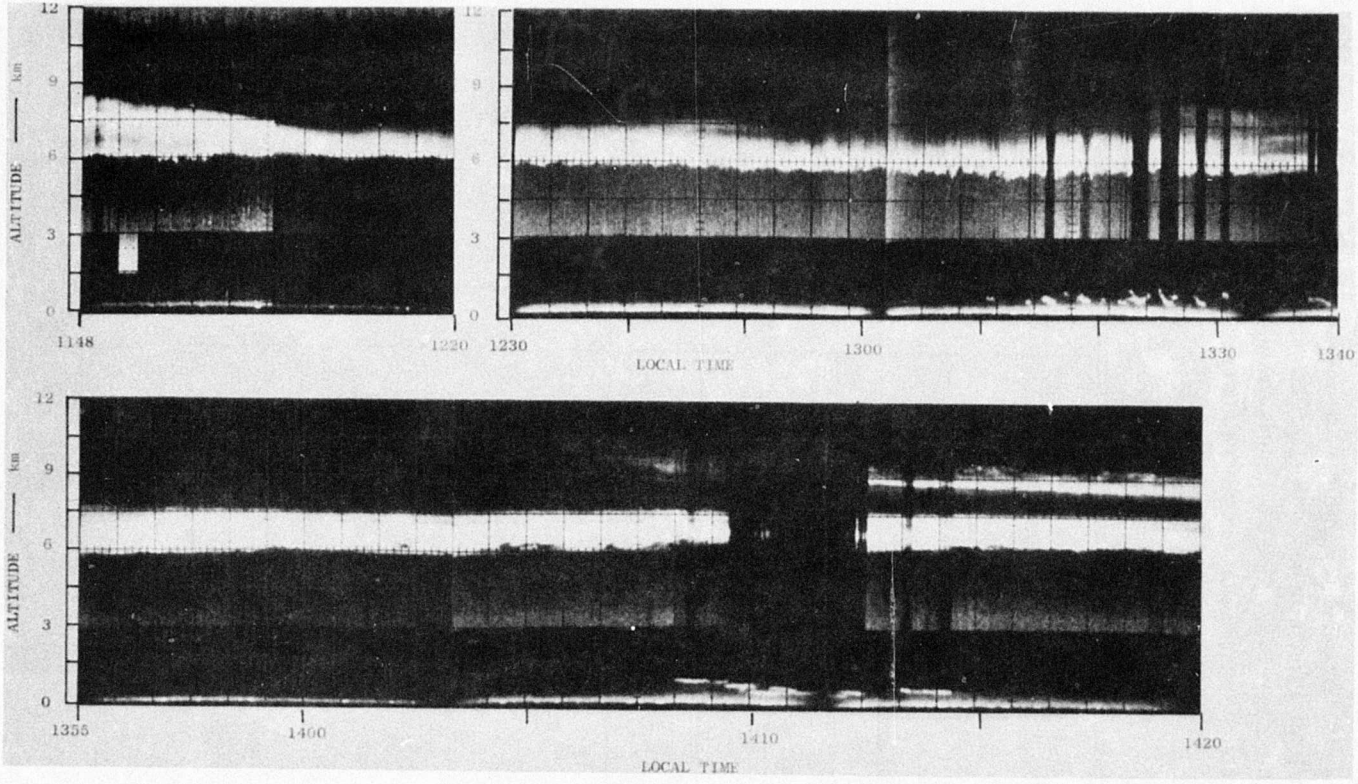

Figure 7. Height-Time Display from the SRI Mark IX Lidar at Gellinam, 0030 to 0220Z, 5 April 1974 (1230 to 1420 local time, 4 April 1974), Courtesy of Uthe et al.[3] Cloud base is near 5.5 km prior to the reentry, and gradually rises to about 6 km at 1400Z. Cloud top heights are consistently below those reported by the WB-57F crew and measured by ALCOR, which implies that the lidar beam is being attenuated by the primary cloud layer throughout the observational period. Particularly strong attenuation is evident at 0050 to 0115Z

On PVM-5 mission day the lidar operated from 2045Z (4 April) to 0429Z (5 April). A cloud layer was detected with a base at 5 to 6 km during the entire period of operation. Polarization measurements indicated that the cloud was predominantly ice crystals, and measured values of the depolarization ratio were consistent with values derived theoretically for backscatter from plate and column crystals. Vertical observations prior to the reentry (Figure 7) showed a fairly uniform cloud layer based at 5.5 km. The cloud top observed by the lidar was generally below 8 km, suggesting attenuation of the lidar beam particularly between 0050 and 0115Z. Elevation scans taken in the reentry corridor at 52° azimuth from Gellinam showed the cloud base height near 5.5 km at 0148Z and increasing to near 6 km at 0154Z. Attenuation due to the longer path length through the cloud layer precluded the determination of the cloud thickness from these scans. Vertical observations taken after the reentry (Figure 7) showed the primary cloud layer between 6 and 7.5 km with minimal variation in structure between 0155 and 0220Z. From a synthesis of the WB-57F photographs (Figure 3) and the soundings (Figure 4) it is evident that the relatively clear area observed from the aircraft passed to the north and west of Gellinam, and thus was not observed by the lidar. Visual observations from Gellinam, however, did note that the clouds seemed lighter at the time of reentry than earlier in the day. Figure 7 also shows an upper cloud layer which was first detected about 0207Z at 10 km altitude. This layer was in the region of southwesterly air flow, and was probably continuous with the upper cloud layer observed from the aircraft. If the lidar beam were being uniformly attenuated by the lower cloud layer during this time, then it is possible that the upper layer was actually present over Gellinam prior to its appearance on the lidar record. Ice water content of the clouds in the reentry corridor determined from the lidar measurements (0.02 to 0.19 gm m^{-3}) was generally consistent with values deduced from the radar and aircraft data, but values deduced from the vertical lidar observations seemed to be too high.

The reentry could not be seen from Kwajalein because of the thick clouds. At Roi-Namur patches of blue sky were visible, as might be inferred from Figure 3, including some in the general direction of the reentry corridor. However, we do not know whether any part of the reentry was actually observed from Roi-Namur.

3. WB-57F WEATHER OBSERVATIONS

Two WB-57F aircraft were at Kwajalein during the period 21 March to 6 April 1974. The operations during that time are summarized in Table 2. Flights prior to launch day were performed for purposes of instrumentation and communications testing, vectoring practice, and cloud sampling. Details of the objectives and accomplishments of all the flights have been provided by MRI.[2]

Table 2. WB-57F Operations at Kwajalein, March-April 1974

Date (1974)	Time (GMT)	Pressure altitude (kft)	(km)	Flight Mode
25 March	0325-0335	20-45	6.1-13.7	Cloud sampling during ascent
		35	10.7	
		30	9.1	Cloud sampling in Kwajalein area
		25	7.6	
	0424-0428	22-35.5	6.7-10.8	Cloud sampling during ascent
26 March	0300-0310	20-45	6.1-13.7	Cloud sampling with MPS-36
	0315-0321	32	9.8	
	0325-0334	28	8.5	Cloud sampling in reentry corridor
	0337-0350	24	7.3	
	0355-0407	20-40	6.1-12.2	Cloud sampling on 058° heading (post-mission simulation)
	0435-0440	28	8.5	Cloud sampling on 135° heading (post-mission simulation)
	0445-0450	26	7.9	Cloud sampling on 270° heading (post-mission simulation)
	0454-0500	22	6.7	Cloud sampling on 360° heading (post-mission simulation)
28-29 March	2355-0002	20-50	6.1-15.2	Mission profile on 058° heading
	0005-0010	46	14.0	Cloud sampling
	0027-0034	46	14.0	
3 April	0400	20-45	6.1-13.7	Initial ascent
		40	12.2	
		38.5	11.7	
		34	10.4	Cloud sampling S of Kwajalein
		32	9.8	
		29.5	9.0	
	0530	16-40	4.9-12.2	Cloud sampling during ascent, SE of Kwajalein
3- 4 April	2333-2343	20-45	6.1-13.7	Initial ascent on 058° heading
	2354-0002	34	10.4	
	0007-0012	32	9.8	
	0019-0027	30	9.1	Cloud sampling in Kwajalein area (over Gellinam)
	0032-0038	28	8.5	
		28	8.5	Cloud sampling 17 km S of Kwajalein
		20-34	6.1-10.4	
		34-20	10.4- 6.1	Cloud sampling SW of Kwajalein
		20-40	6.1-12.2	
		40-25	12.2- 7.6	
	0207-0214	30	9.1	Cloud sampling over lagoon

Table 2. WB-57F Operations at Kwajalein, March-April 1974 (Contd)

4 April (cont)	0304-0310	37	11.9*	Cloud sampling with MPS-36 and ALCOR in link-offset mode
	0313-0318	35	11.5*	
	0323-0330	33	10.7*	
	0335-0340	31	10.0*	
	0343-0350	29	9.5*	
	0356-0403	27	8.8*	
	0408-0412	25	8.1*	
5 April	0025-0036	20-45	6.1-13.7	Ascent on 058° heading in reentry corridor
	0037-0052	45-20	13.7- 6.1	Descent on 238° heading
	0122-0134	22	6.7	Cloud sampling on 058° heading
	0152-0159	52.5	16.0	Photo-mapping run
	0236-0245	20-45	6.1-13.7	Post-mission ascent in reentry corridor
	0300-0305	40	12.9*	Cloud sampling with MPS-36 and ALCOR in link-offset mode
	0308-0312	37.5	12.1*	
	0314-0320	35	11.4*	
	0323-0335	32.5	10.5*	
	0343-0347	30	9.7*	
	0355-0401	27.5	9.0*	
	0404-0410	25	8.1*	
	0414-0419	22.5	7.3*	
	0422-0429	20	6.6*	

*Altitude determined from ALCOR tracking data

Weather data were recorded in conjunction with ALCOR in the link-offset mode on 4 and 5 April. There was significant weather on both of these days, and the data from 5 April have been presented by Barnes et al.[4]

Cloud physics instrumentation was housed principally in two removable pods mounted near the outer end of each wing, as shown in Figures 8 and 9. These are described in detail by Jahnsen et al.[2] The principal instruments were the PMS probes, which measured particle sizes in the ranges 1 to 31 μm (axially scattering spectrometer), 28 to 310 μm (optical array cloud particle spectrometer), and 140 to 1907 μm (optical array precipitation spectrometer).* Each spectrometer recorded particle counts in fifteen channels. A Formvar particle replicator (MRI Model 1203B) provided a continuous record of the types of hydrometeors encountered by the aircraft. Images of particles greater than 2 μm in length were preserved in an adhesive resin applied to a 16-mm sampling tape. These data

*These are the outer limits of the measured sizes, rather than the ranges of the channel center diameters.

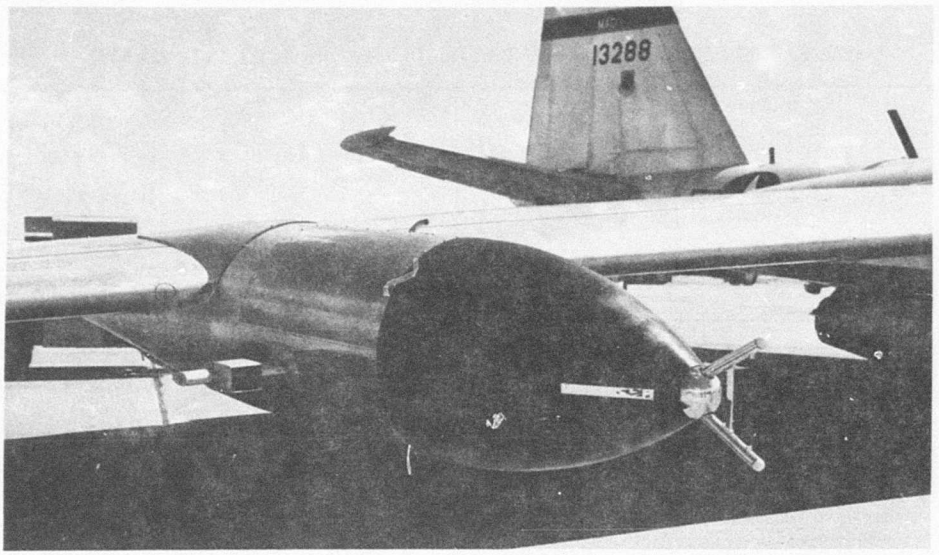

Figure 8. Instrumentation Pod on Right Wing of WB-57F Aircraft. Precipitation spectrometer is at the forward end of the pod, and MRI replicator is on the side

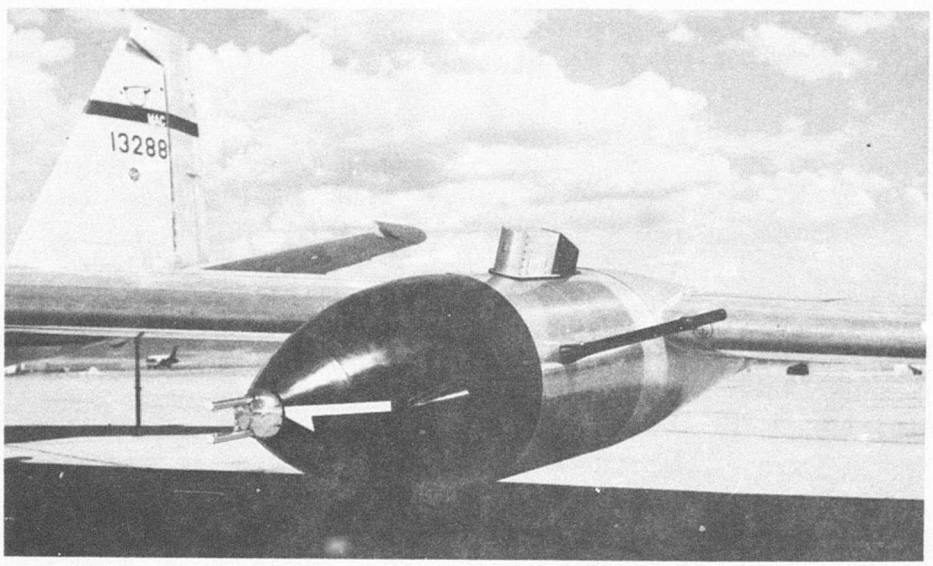

Figure 9. Instrumentation Pod on Left Wing of WB-57F Aircraft. Cloud particle spectrometer is at the forward end, axially scattering spectrometer is on the side, and MRI foil sampler is on the top

are essential to the analysis of the PMS data, as the computation of ice water content and reflectivity from the one-dimensional size spectra requires an approximation of the crystal habit. A second hydrometeor sampler (MRI Model 1220 foil impactor) recorded images of particles greater than 250 μm in size on a thin metallic film. Additional instrumentation measured temperature, pressure altitude, and indicated airspeed, which were recorded along with observations by the crew. MRI was responsible for the cloud physics instrumentation described above, and EG&G operated the on-board tape recorders.

A holographic camera developed and operated by SAI[9] was installed on the WB-57F fuselage. This system utilizes a pulsed ruby laser to produce holograms of a sample volume 5 cm in diameter and 15 cm long at a rate of 3 per minute. A three-dimensional image of the sample volume can be reconstructed from each hologram, and individual crystals can be observed with a resolution of about 50 μm. Unfortunately, due to failure of a capacitor bank and other technical problems, very few holograms were obtained during this operational period at Kwajalein, and none during the correlation flights on 4 and 5 April.

The WB-57 F's were equipped with forward- and downward-looking cameras which were used to supplement the other sensors. The downward-looking F415P camera was used only during the pre-impact high-altitude photo-mapping run, as described in Section 2.

The pre-impact observations from the aircraft are described in Section 2. Following the reentry the aircraft made an ascent in the corridor starting at 0236Z. Maximum ice water content observed during the ascent was 0.035 gm m^{-3}, at 7.5 and 8.5 km. The forward-looking camera indicated that the aircraft was in clouds most of the way up, although the crew reported that they were in the clear at 9 to 10 km altitude and could see a cirrus layer above, near 12 km.

Correlation operations with ALCOR were conducted between 0300 and 0430Z, following the flight patterns shown in Figure 10. The PMS and ALCOR data recorded during these operations were presented by Barnes et al.,[4] with a description of the analysis technique. The Z-M equations derived from these data are summarized in Section 4. The cloud structure observed by the aircrew and recorded by the forward-looking camera is presented here, as it was not described in detail by Barnes et al.[4] The WSR-57 scans during this period, shown in Figure 11, indicate that there was less convective shower activity than at the time of reentry. One cell, about 30° azimuth and 50 to 60 km range at 0310Z, passed through the sampling area during the operations.

---

9. Trolinger, J.D., Farmer, W.M., and Clayton, F.P. (1974) Development and Application of an Airborne Holography System and Particle Sizing Interferometer, SAI-74-511-TT, Science Applications, Inc., La Jolla, Calif.

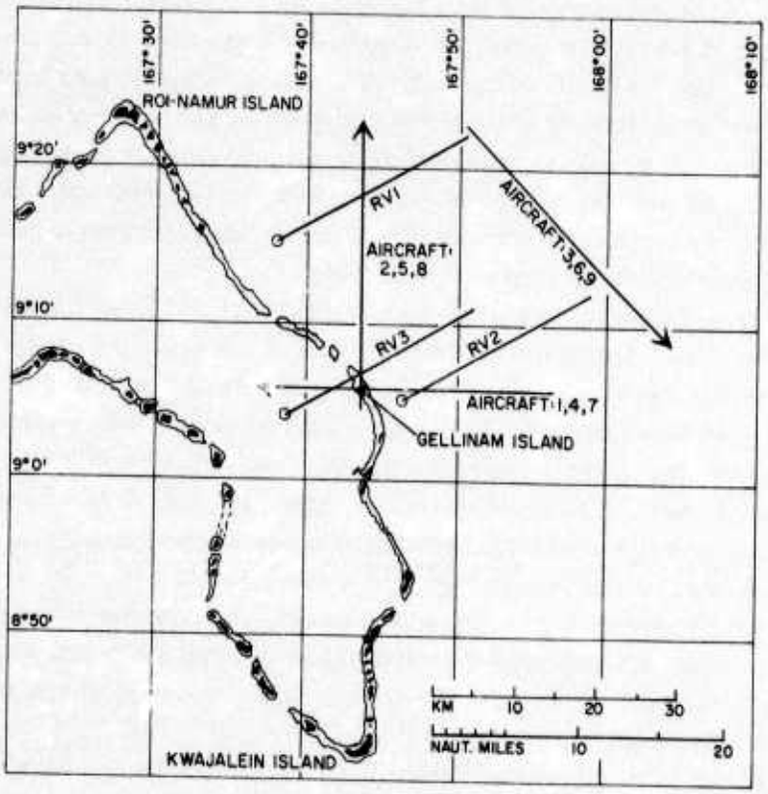

Figure 10. Flight Tracks for Correlation Operations and PVM-5 Reentry Trajectories. Flight tracks are numbered starting with the uppermost at 12.9 km altitude. Criteria for establishing these tracks were (1) that they be in the reentry corridor, (2) that some should pass over the SRI lidar at Gellinam, and (3) that the aircraft and the ALCOR tracking gate not be at the same slant range from ALCOR, so as to eliminate side-lobe echoes from the aircraft

On the first pass at 12.9 km the WB-57F was near the top of the clouds. Blue sky could be seen above the aircraft, but the horizon was indistinct, indicating that they were just into the clouds. Some particle counts were observed, but the radar reflectivity values were close to the ALCOR system noise level. The second pass, heading north at 12.1 km, was in clouds, but seemed to move into less dense clouds toward the end. The pilot noted that they were passing near a convective buildup just east of the flight path. The third pass, at 11.4 km, was between two cloud layers, and the aircraft was in the clear most of the time. The fourth pass, heading west at 10.5 km, was in clouds most of the distance. It was extended over the lagoon in an attempt to penetrate some convective cells in that area, but the aircraft broke out of the clouds in the last three minutes of the pass. At this time the aircraft again appeared to be between

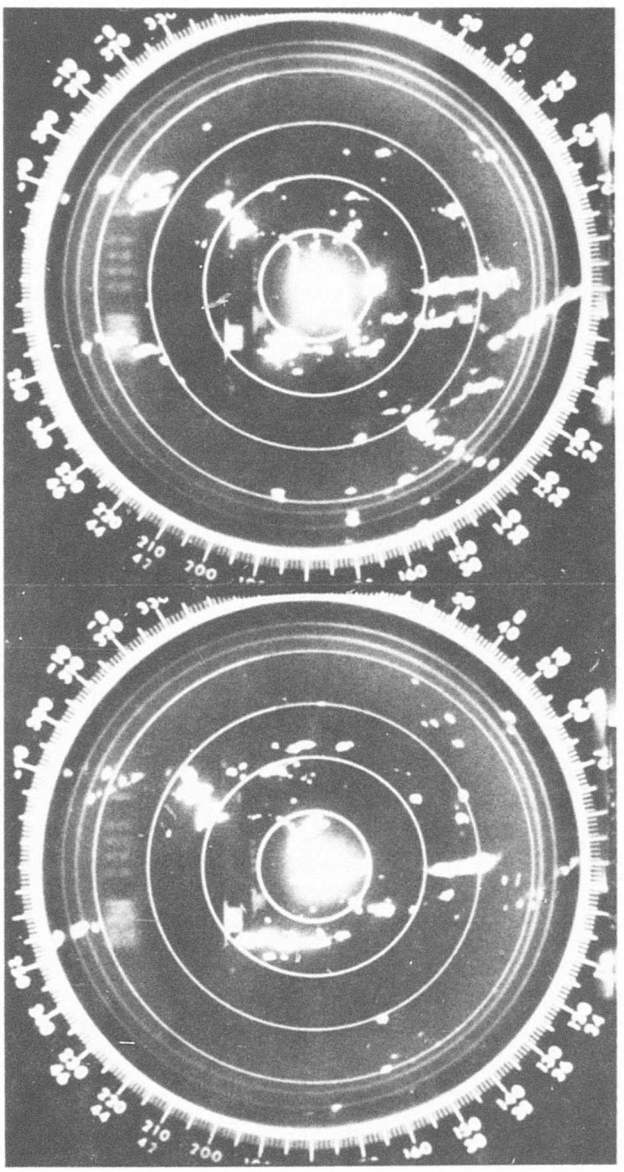

Figure 11. WSR-57 Radar PPI at 0310 and 0340Z, 5 April 1974. Format is identical to that of Figure 6. Shower activity is less at this time than during the reentry, but several cells are moving through the area of the correlation sampling operations

two cloud layers, and a convective top could be seen protruding through the lower layer. This may have been the same cell noted in conjunction with Pass 2 above, or the cell seen in Figure 11 at 340° azimuth and 85 to 90 km range from Kwajalein at 0340Z. The five lowest passes were in clouds continuously, and the pilot reported seeing precipitation on the canopy during Passes 6 and 9. This observation is consistent with the relatively large values of water content deduced from the PMS data for these passes.

The replicator tapes indicated that the crystals were predominantly plates at all altitudes. The PMS data were initially analyzed on the assumption of 100 percent single plate crystals at all altitudes. Subsequently MRI determined that an approximation of 75 percent aggregates of plates and 25 percent single plate crystals was more appropriate for the lowest three passes. The derived values of ice water content are increased slightly by this change in crystal habit approximation, but these data are not presented in detail here. Correlations of Z and M based on both sets of data are shown in the following section.

4. ALCOR WEATHER OBSERVATIONS

Weather support operations at KREMS were conducted throughout the time that the Weather Team was at KMR. These operations are summarized in Table 3. Two innovations in technique provided significant improvement in the correlation of aircraft and radar measurements and permitted the use of quantitative radar data for pre-mission computation of M and WSI profiles for forecasting. The first of these was the link-offset mode, whereby the MPS-36 aircraft track file was transmitted through the CDPC to the PRESS computer, offset by a vector (normally 3 km) in the direction of the aircraft flight, and used to control ALCOR while the weather data were being recorded. The offset distance was later removed as part of the data analysis procedure, described by Barnes et al.[4] The second innovation involved the use of radar cross-section data recorded in real time at the PRESS computer for generating reflectivity and water content profiles. These data, recorded on a tape designated "B-6," enabled us to compute one-second averages of cross section, and meteorological quantities, at the tracking point of the radar. Possible radar track files included nominal reentry trajectories (from the mission Real Time Programs), vertical scans over designated points, and the link-offset track file of the WB-57F. The vertical scans could be made through particular features of the weather, or at points upwind from the trajectories for advection forecasting of WSI on the trajectories. The details of the B-6 data processing are described in Appendix A.

Table 3. ALCOR/PRESS Weather Support, March-April 1974

25 March	PRESS Program modifications
26 March	RHI scans at 0135, 0142Z Vertical weather scan at 0148Z (No detectable weather)
26 March	RHI scans at 2115, 2118Z Vertical weather scan at 2127Z (No detectable weather)
28 March	Vertical scans at 2054, 2229Z (No detectable weather)
1 April	PRESS Program modifications
3 April	RHI scan at 0213Z Vertical scan at 0245Z (Minimal weather)
3 April	RHI scans at 2100, 2236Z Vertical scans at 2107, 2247Z (Weather approx. 6-12 km) Trajectory scans at 2129-2133Z (WSI* 0.4, 0.5, 0.3, for RV1,2,3)
4 April	RHI scans at 0003, 0016, 0039, 0120, 0240Z Vertical scans at 0014, 0053Z (WSI* = 1.6, 7.2)
	Aircraft correlations — Alt (km) — Hdg (deg) 0308:53-0310:15 — 11.9 — 000 0312:54-0318:35 — 11.5 — 135 0323:00-0325:55 / 0326:25-0330:38 — 10.7 — 270 0335:15-0339:56 — 10.0 — 000 0343:23-0349:55 — 9.5 — 135 0355:32-0402:59 — 8.8 — 270 0407:56-0411:40 — 8.1 — 000
4 April	RHI scans at 2030, 2058, 2227, 2237, 2312, 2350Z
	Vertical scans — Cld Base (km) — Cld Top (km) — WSI* 2107 — 5.0 — 12.3 — 16.9 2236 — 4.5 — 12.1 — 8.3 2313 — 4.2 — 11.1 — 4.6 2352 — 5.6 — 10.5 — 2.5 Trajectory scans 2132-2136 — 3-5 — 11-12 — 3.1 (RV2)

*WSI computed from Eqs. (3) and (7)

Table 3. ALCOR/PRESS Weather Support, March-April 1974 (Contd)

5 April	RHI scans at 0030, 0315, 0322, 0420Z			
	Vertical scans	Cld Base (km)	Cld Top (km)	WSI*
	0030	5.7	12.7	2.9
	0126	5.7	13.0	4.0
	Post-impact scans			
	0154:02-0155:05	5.9	9.4	RV3
	0155:22-0156:25	6.5	12.0	RV1
	0156:41-0157:45	5.7	8.6	RV2
	0158:01-0158:12			Vertical
	0158:45-0159:48	6.1	9.3	RV3
	0200:05-0201:08	6.3	12.5	RV1
	0201:25-0202:28	3.9	10.1	RV2
	0202:45-0202:56			Vertical
	0203:14-0204:17	6.2	9.8	RV3
	0204:33-0205:37	6.5	12.7	RV1
	0205:53-0206:57	4.3	10.6	RV2
	0207:13-0207:24			Vertical
	Aircraft correlations	Alt (km)	Hdg (deg)	
	0259:59-0305:49	12.9	270	
	0309:11-0312:23	12.1	000	
	0314:26-0320:10	11.4	135	
	0322:50-0335:24	10.5	270	
	0343:19-0347:38	9.7	000	
	0355:11-0401:26	9.0	135	
	0404:16-0410:42	8.1	270	
	0414:00-0419:18	7.3	000	
	0421:55-0428:59	6.6	135	

*WSI computed from Eqs. (3) and (7)

In addition to the data recorded on the B-6 tape, data were recorded at ALCOR in the same manner as for previous missions. The ALCOR data tapes were processed by Lincoln Laboratory and provided to AFCRL with calibrated radar signal values at 170 range gates spaced across a 2.5-km data window. These yielded a two-dimensional view of the weather structure along the trajectories. The complete radar weather data flow is shown in Figure 12. Weather scans were made with ALTAIR UHF for the purpose of identifying backscatter signals from clear-air fluctuations of the refractive index. However, no atmospheric echoes could be seen on the ALTAIR RTI films from these scans. ALTAIR VHF (193-cm wavelength) was not used for weather data.

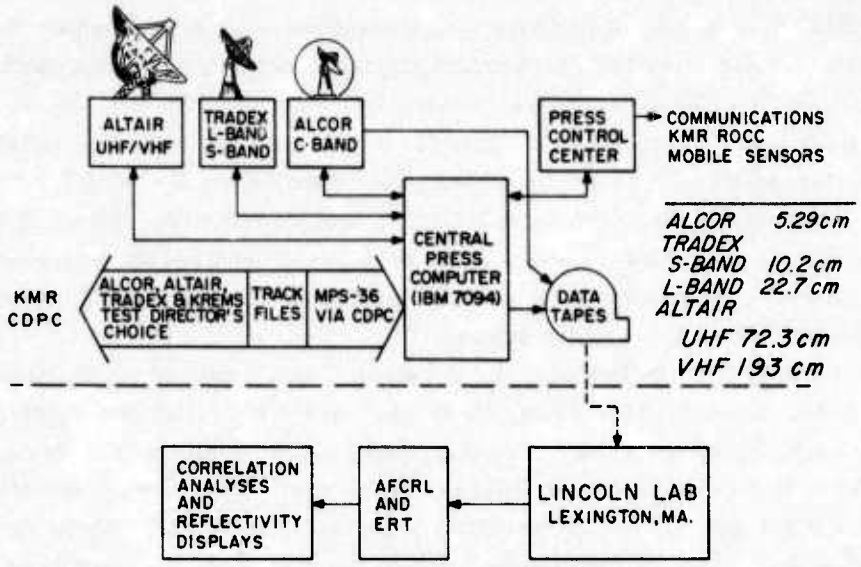

Figure 12. Radar Weather Data Flow Diagram. ALCOR is the principal weather sensor, with TRADEX S-band as backup. ALTAIR UHF is intended to provide additional data on clear-air echoes, with TRADEX L-band as backup. ALCOR data are recorded on the PRESS B-6 tape for on-site processing of 1-sec averages, and also recorded directly for later processing at Lincoln Laboratory. Final processing and analysis are done by ERT programmers and AFCRL scientists

The reflectivity factor Z ($mm^6\ m^{-3}$) was computed by the equation

$$Z = C\sigma/r^2 , \tag{4}$$

or

$$dBZ = 10 \log C + 10 \log \sigma - 20 \log r , \tag{5}$$

where σ is the cross section (m^2), r is the range (km), and

$$C = \left[\frac{\lambda^4 \times 10^{10}}{\pi^5 \times |K|^2}\right]\left[\frac{8 \ln 2}{\pi\theta^2 h \times 10^6}\right] \tag{6}$$

where λ is the wavelength (5.30 cm), h is the pulse length (37.5 m), θ the beamwidth (5.24×10^{-3} rad), and $|K|^2 = 0.197$ for radar backscatter from ice crystals and 0.93 for backscatter from rain. Because ALCOR transmits a frequency-modulated "chirp" pulse, the pulse length used in the above computation is not the

transmitted pulse length but rather a compressed pulse length corresponding to the output of a pulse-compression network in the radar receiver. Comparisons of chirp and constant-frequency radar weather data from the TTR-4 radar at Kwajalein[8] showed that the computational factor determined from Eq. (6) above had to be increased by 3 dB for the chirp data. Thus 10 log C = 86.5 for the ALCOR observations above the freezing level, and 79.8 in rain. We used only the values from the left circular polarization (opposite to the transmitted polarization) for this analysis, as these are 15 to 20 dB greater than those received on right circular polarization for weather echoes.

The quantity Z is the factor of the received signal power which is dependent only on meteorological parameters. It is equal to the sixth moment of the particle size spectrum, and thus is not a direct measure of the water content which is proportional to the third moment, that is, the volume. The relation of reflectivity to water content depends on the spectrum of ice crystals or water drops in a cloud. For final interpretation of the reflectivity profiles measured along the trajectories we used the Z-M equations shown below. For preliminary estimates of water content, used for pre-mission forecasting and for the quick look post-mission briefing, we used a Z-M equation appropriate to ice crystals:[10]

$$M = 0.038\, Z^{0.529}, \tag{7}$$

above the freezing level. Below the freezing level we used a Z-M equation appropriate to tropical rain:

$$M = 0.011\, Z^{0.43}, \tag{8}$$

derived from equations presented by Battan.[11] (It should be noted that this Z-M equation was derived from surface observations and is therefore not strictly applicable to observations in clouds; however, it is useful for preliminary estimates of the cloud water content.)

Qualitative vertical cross sections of the weather structure were generated by means of the SPA-40 RHI display unit at KREMS. During the pre-mission period scans were made in the southwest quadrant so as to monitor the weather upwind from the reentry corridor (based on the 2100Z sounding which showed westerly or southwesterly winds between 7.3 and 12.5 km). These scans were used to select coordinates for the pre-mission vertical WSI scans, which provided

10. Heymsfield, A.J. (1973) The Cirrus Uncinus Generating Cell and the Evolution of Cirriform Clouds, PhD Thesis, The University of Chicago.

11. Battan, L.J. (1973) Radar Observation of the Atmosphere, Univ. of Chicago Press, 324 pp.

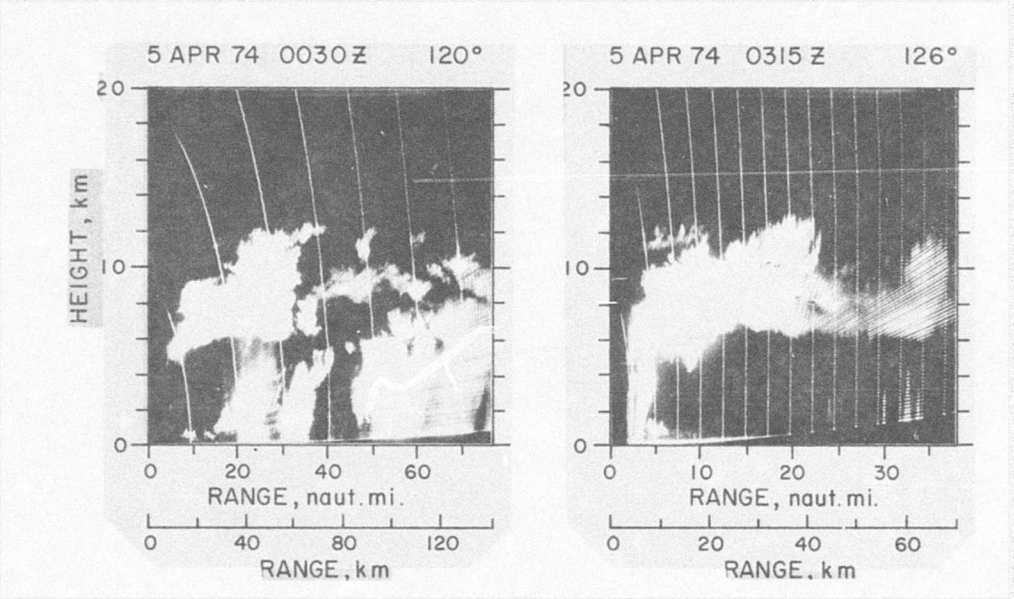

Figure 13. ALCOR RHI Scans During PVM-5 Operations. Range markers are at intervals of 5 nmi (9.3 km). Both scans show the primary cloud layer between 6 and 12 km, with peaks suggesting convective activity reaching to nearly 13 km. Low-level showers are present below 6 km, particularly during the 0315Z scan. A separate upper cloud layer, as is observed on the RV1 trajectory scans, is present at 11 to 12 km altitude out to 40 km range at 0030Z

short-term forecasts of the reentry corridor weather. The early scans showed a thick layer between 5 and 11 km, with some showers embedded in it, and showers below 5 km. A scan at 0030Z toward the southeast, in the general direction of the reentry corridor, is shown in Figure 13. The base of the layer at this time had risen to about 6 km, but echo tops extended to 13 km. This layer persisted through the time of the aircraft correlation sampling, with heavy showers below 6 km at times, as shown in Figure 13. The RHI scan at 0315Z suggested that the layer was beginning to break up, but a scan at 0420Z, near the end of the correlation sampling, showed the layer between 6 and 12 km altitude extending to more than 100 km range.

Radar weather data along the three reentry trajectories are shown in Figures 14 through 19. A scan was made down the RV3 trajectory just prior to impact. Following the reentry, a sequence of scans was made, once down each trajectory from about 20 km to near 1 km and once vertically over the radar from 6 to 20 km, and repeated three times. The sequence of scans on each trajectory provided a time history of the weather along the trajectory. The vertical scans were intended to reveal high thin layers which might be too weak to appear in the

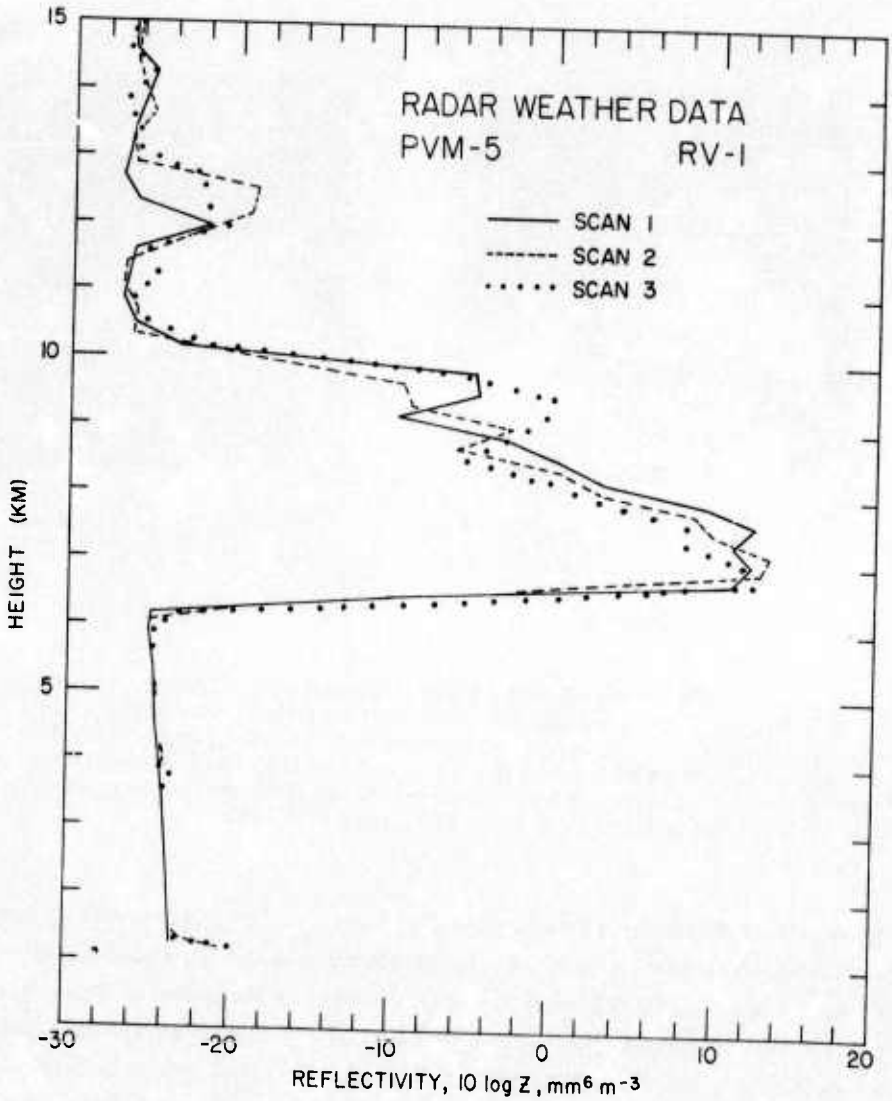

Figure 14. Profiles of Radar Reflectivity Factor Z on PVM-5 RV1 Trajectory. These are derived from the PRESS B-6 data and presented in logarithmic form, with Z expressed in $mm^6\ m^{-3}$, illustrating the changes in the weather structure during 9 minutes following the reentry. Interpretation of these data in terms of water content is shown in Figure 22. Values above 13 km and below 6 km correspond to the radar system noise level (minimum detectable reflectivity)

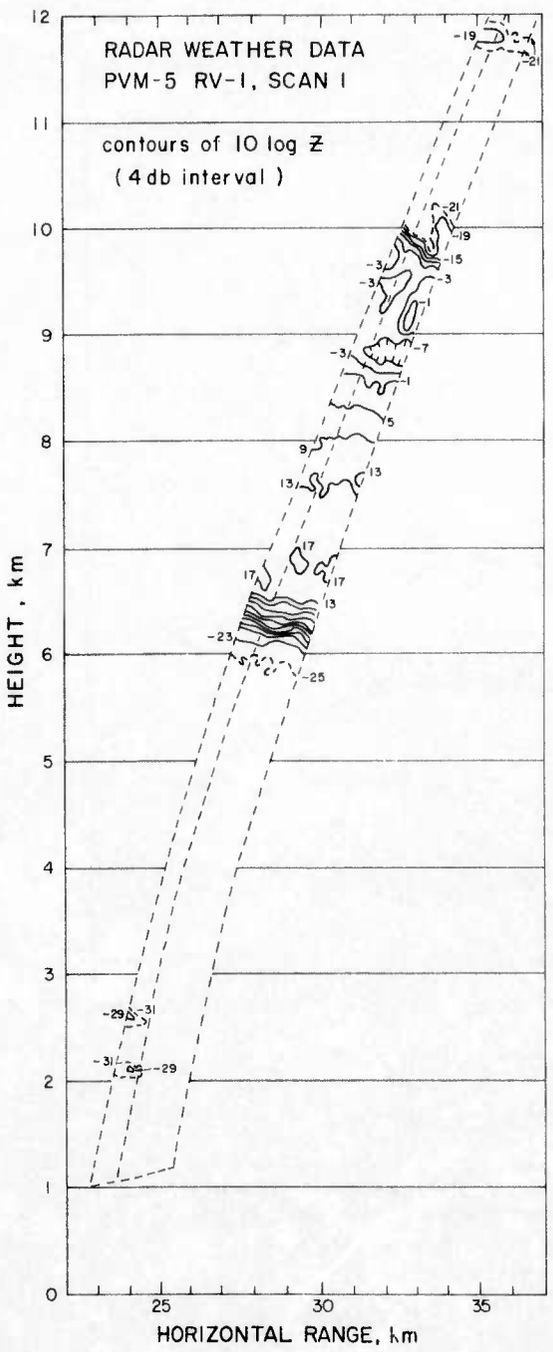

Figure 15. ALCOR Scan of PVM-5 RV1 Trajectory at 0156Z, 5 April 1974. Contours are of 10 log Z, with Z in $mm^6\ m^{-3}$. These values were derived from the original ALCOR data recorded across a 2.5-km interval in slant range. Nominal trajectory location is approximately 1/3 of the width of the array from the near-range side. Irregular structure of the layer top near 10 km is probably associated with embedded convective activity; later scans show more horizontal uniformity

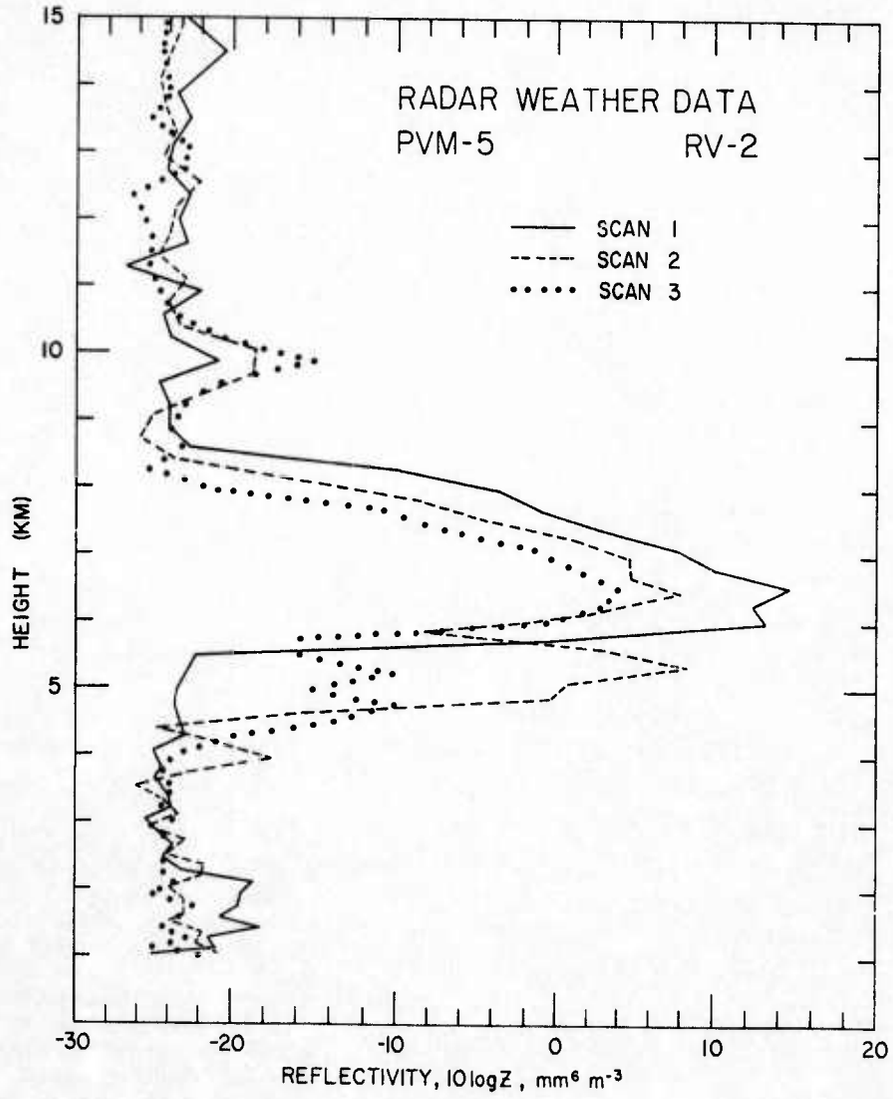

Figure 16. Profiles of Radar Reflectivity Factor Z on PVM-5 RV2 Trajectory. See text and legend of Figure 14 for details

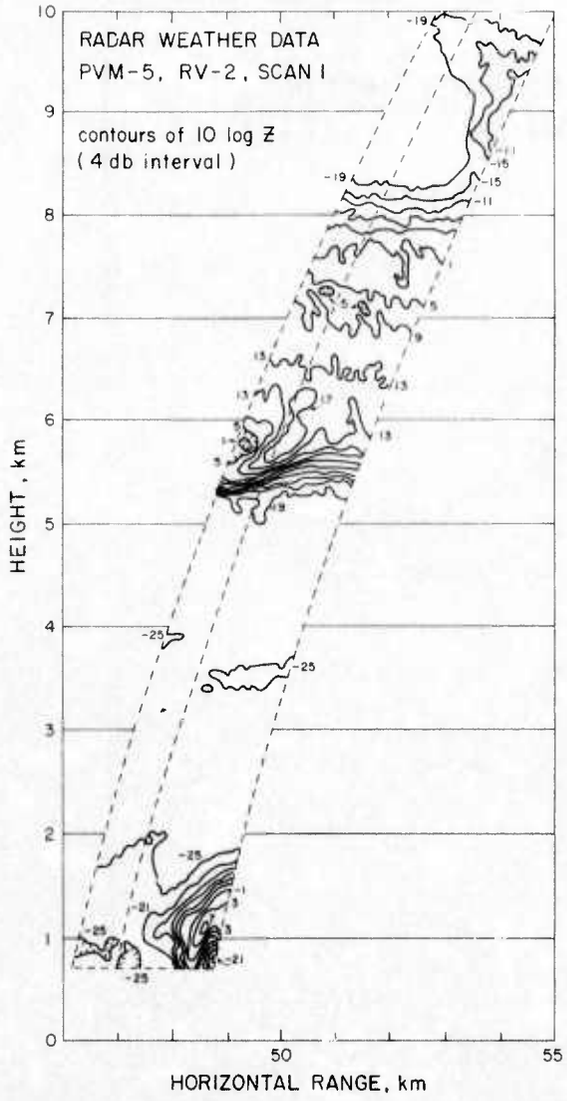

Figure 17. ALCOR Scan of PVM-5 RV2 Trajectory at 0157Z, 5 April 1974. Format is identical to that of Figure 15. Echo structure above 9 km suggests a spreading cumulus top, which is increasing in intensity during the post-impact scans. Strongest echo, near 6 km, is due to a precipitation cell moving through the trajectory area; successive scans show this cell moving to the far side of the data window and disappearing from view. Shower below 2 km is moving toward the west with the low-level winds, and only the edge is encountered by the reentry vehicle

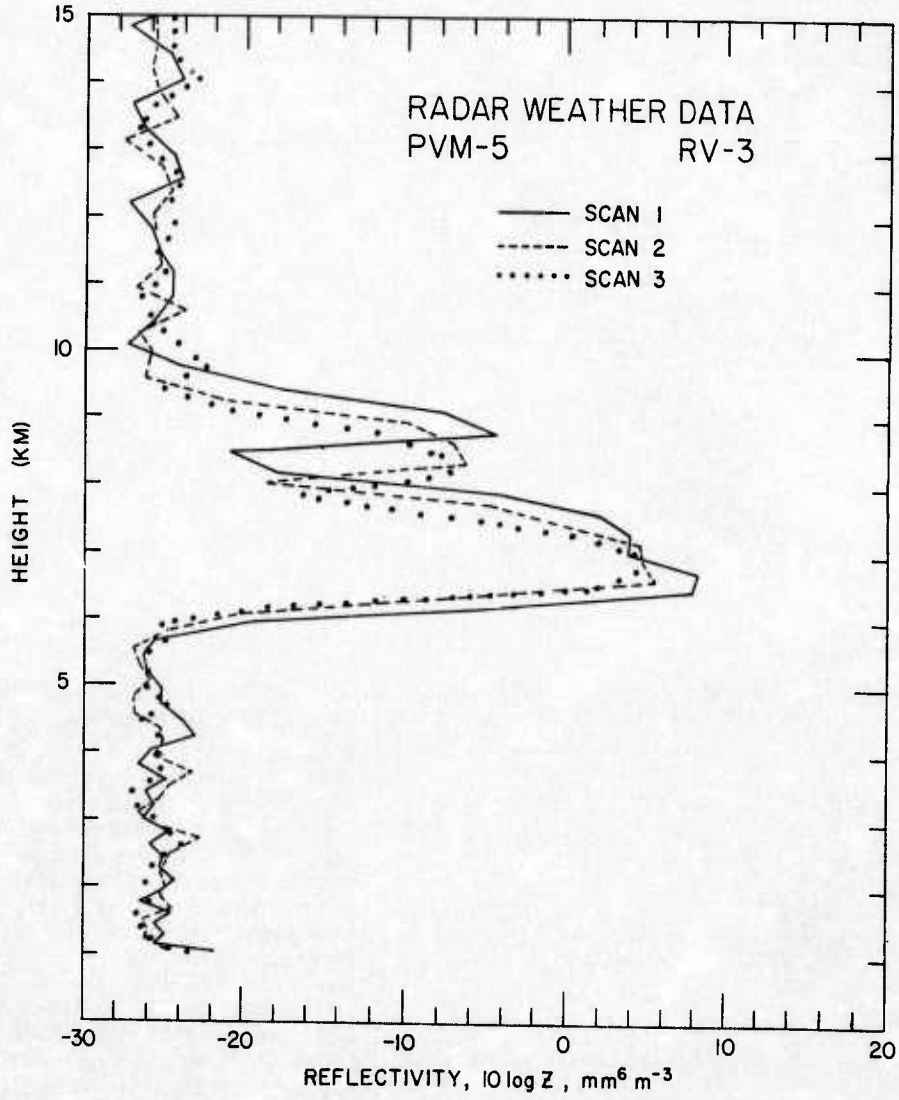

Figure 18. Profiles of Radar Reflectivity Factor Z on PVM-5 RV3 Trajectory. See text and legend of Figure 14 for details

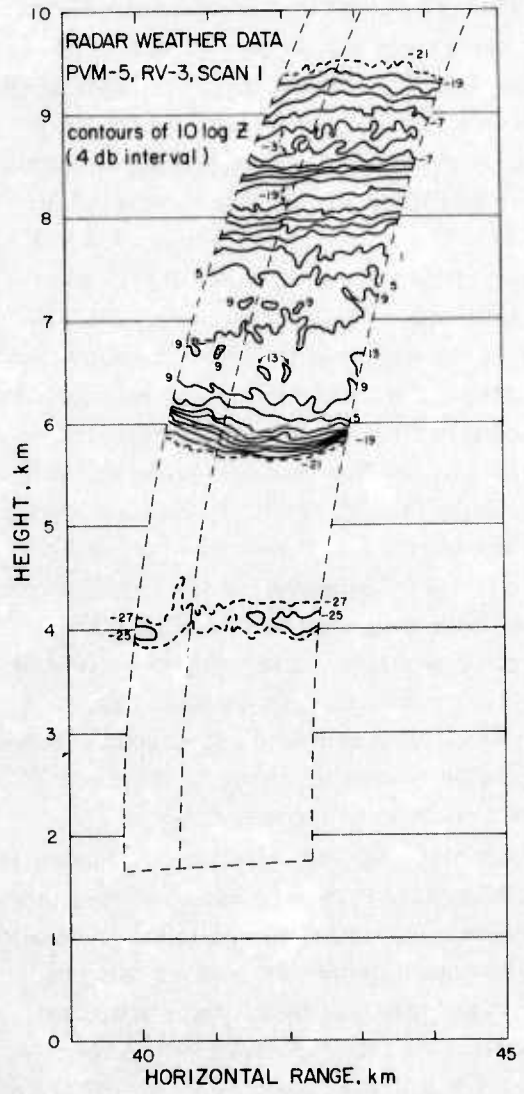

Figure 19. ALCOR Scan of PVM-5 RV3 Trajectory at 0155Z, 5 April 1974. Format is identical to that of Figure 15. Weather structure is the most horizontally uniform of any of the trajectories. Pre-impact scan and post-impact scan 3 (0204Z) show weak echoes near 12 km altitude at the far side of the window, indicating the presence of the high cirrus layer that is also evident in the RV1 and vertical scans

trajectory scans, since the minimum detectable signal level increases as the square of the slant range.

The profiles in Figures 14, 16, and 18 were derived from the B-6 data, and show the changes of the reflectivity structure during the few minutes after the reentry. The primary cloud layer was between 6 and 10 km on the RV1 trajectory (Figure 14) with some evidence of a double layer structure. A secondary layer was detected between 11.5 and 13 km and exhibited considerable variation in thickness and intensity during these scans. This RV passed through the thick clouds that were between Gellinam and Roi-Namur (Figure 3). Figure 15 shows the relatively uniform structure of the clouds close to the trajectory. Changes in the upper part of the cloud layer, between 8.5 and 10 km, accompanied a tendency toward more horizontal uniformity in the later scans. The sharp temporal variations of the RV2 weather structure, shown in Figure 16, are due to particular features of the weather shown in Figure 17. The intense echo between 5.6 and 6.3 km, probably from a convective shower imbedded in the cloud layer, was advecting through the trajectory during the scans. The tilt of this cell was approximately consistent with the direction of the wind shear (toward the south) just below the height of the maximum northeasterly flow (Figure 4). The motion of the cell did not seem to correspond to the strong northeasterly flow shown in the soundings, but possibly was being controlled by the flow near the top of the cell, where the wind was backing from northeasterly through northerly (to southwesterly above 7 km). The decreasing top height and intensity of the primary cloud layer was undoubtedly associated with the approach of the relatively clear area observed from the WB-57F. The uppermost part of the cloud, between 9 and 10.5 km, appeared to be evolving independently of the lower layer, becoming more intense but retaining its asymmetrical structure during the successive scans. The trajectory passed through the edge of the small shower below 2 km, but the reflectivity levels indicated in Figure 16 imply water content less than 0.002 gm m^{-3} with Eq. (8). The RV3 trajectory yielded the lowest values of reflectivity (Figure 18), probably due to its proximity to the relatively clear area. Figure 19 shows that the weather was more horizontally uniform than on the other trajectories, and it showed a consistent trend of decreasing top height and intensity of both layers. The vertical scans (Figure 20) show multiple weather echoes between 5 and 10 km, with peak reflectivities somewhat less than those observed on the trajectories. These clouds, however, were not continuous with those in the reentry corridor, as can be seen in Figure 3. The upper layer, at 11.4 to 12.7 km, gave reflectivity similar to the uppermost layer on the RV1 trajectory. It is likely that this layer extended across all the trajectories, although it was below the minimum detectable signal level on the RV2 and RV3 trajectories. With this

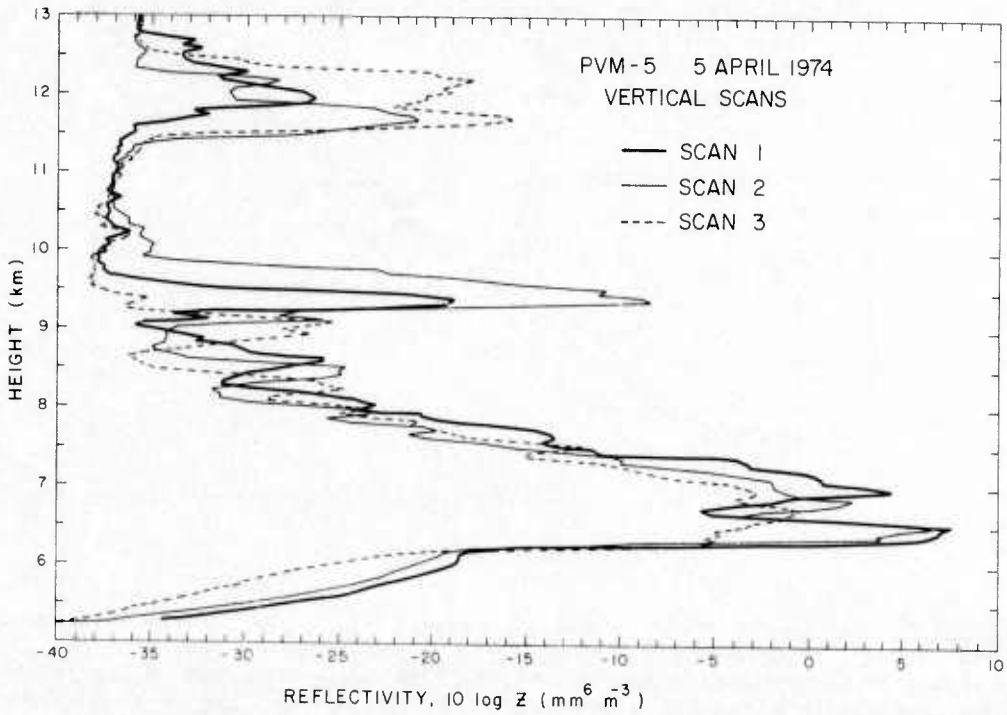

Figure 20. Profiles of Reflectivity Factor Z on ALCOR Vertical Scans at 0158 to 0207Z, 5 April 1974. Primary cloud layer, between 5 and 8 km, is of lower density than those on the trajectories; Figure 3 shows that this is actually a separate cloud mass. Weak echoes between 8.3 and 9.5 km are probably part of the primary cloud layer. Upper layer at 11.4 to 12.7 km is part of the cirrus layer covering the entire reentry area

exception, we consider the first post-impact trajectory scans to be representative of the weather actually encountered by the reentry vehicles.

Radar weather data were recorded in conjunction with the WB-57F utilizing the link-offset mode described above. The cloud structure observed from the aircraft is described in Section 3, and the radar data are presented in detail by Barnes et al.[4] The Z-M equations derived from their analysis are shown in Figure 21. Correlations derived from the re-analyzed PMS data (using 75 percent aggregates of plate crystals) are included in Figure 21 for comparison. This re-analyzed PMS data (using 75 percent aggregates of plate crystals) are included in Figure 21 for comparison. This re-analysis did not change the trajectory water content profiles significantly.

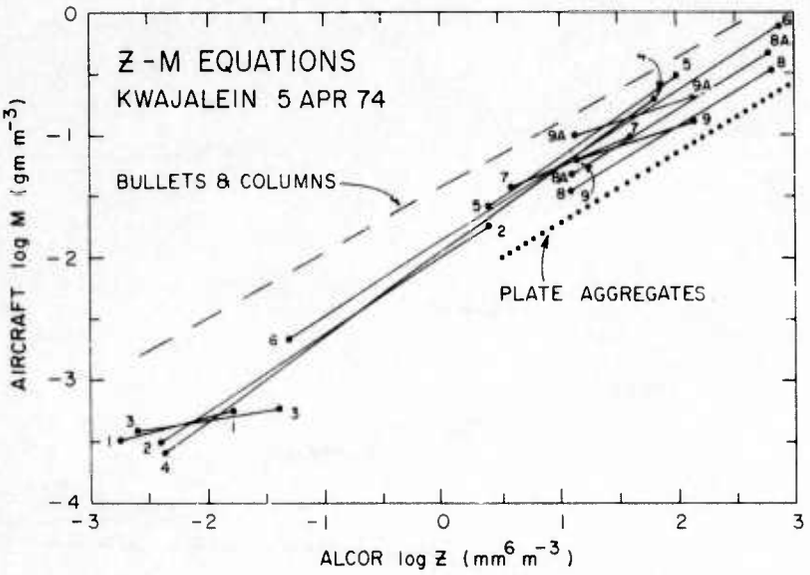

Figure 21. Composite of Z-M Equations Derived from PVM-5 Aircraft and Radar Weather Data. Equations are numbered sequentially from the highest altitude. Re-analyzed correlations based on modified PMS data are labeled 8A and 9A. Equations appropriate to bullet and column crystals (Eq. 7), measured in continental U. S. cirrus, and plate aggregates, measured at Wallops Island, Va., are shown for comparison

5. SUMMARY AND CONCLUSIONS

The water content profiles encountered by the PVM-5 reentry vehicles are shown in Figure 22. These were derived from the post-impact radar scans of the trajectories by means of the Z-M equations shown in Figure 21, and are accurate to about 3 dB (a factor of 2). The profiles presented by Jahnsen et al.[2] are in good quantitative agreement with those in Figure 22 with respect to the maximum values of ice water content. The aircraft did obtain values of ice water content greater than 0.003 gm m^{-3} above 12 km on the post-mission ascent, but these were probably due to a large convective cell near the flight path. The weather pattern that produced these clouds developed over a period of several days, but within the large-scale pattern there were local convective cells and relatively clear areas, which resulted in rapid local changes in the cloud structure. There were some indications that the widespread cloudiness was beginning to break up, at least in the Kwajalein area, about the time of the test, but the clouds persisted sufficiently that the WB-57F and ALCOR obtained good correlation data about 1 to 2-1/2 hours after the reentry.

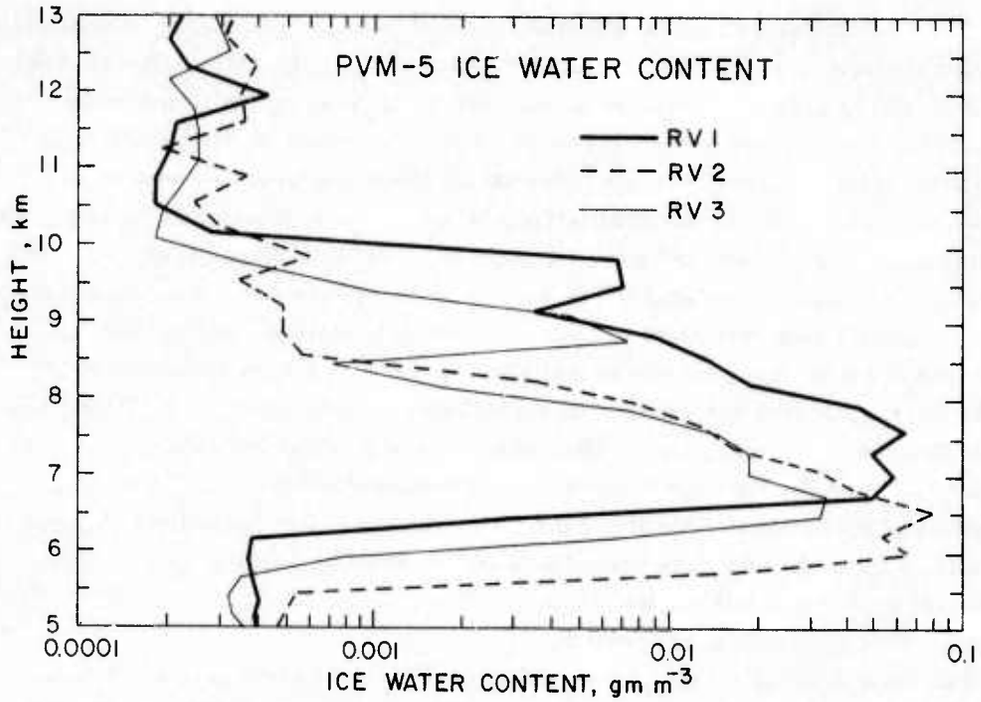

Figure 22. Profiles of Ice Water Content on the PVM-5 Trajectories. These are derived from the radar reflectivity profiles (Figures 14, 16, and 18) by means of the Z-M equations shown in Figure 21. Peak values of M and height of the cloud base agree with corresponding features derived from WB-57F soundings before and after the reentry

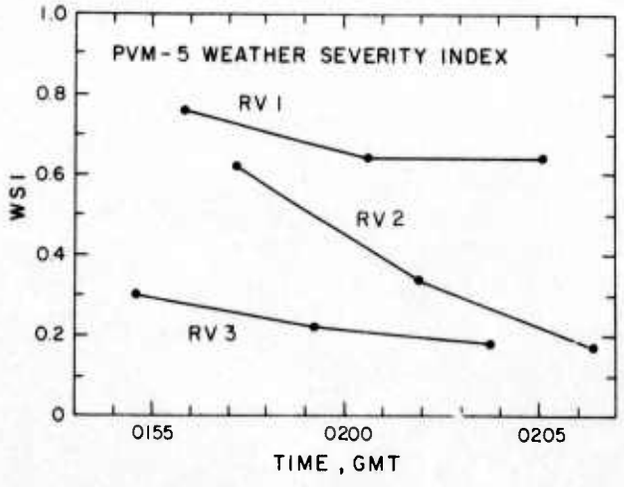

Figure 23. Variations of WSI During the PVM-5 Trajectory Weather Scans. Derivation of these values is as described for Figure 22. Time-history provides a measure of the accuracy of the definition of the WSI actually encountered by the reentry vehicles

The principal uncertainties affecting these results are the rapid changes of the weather on the trajectories and the uncertainties of the PMS data analysis. MRI reported WSI of 1.91 for an ascent 80 min before impact, and 0.65 for an ascent 50 min after impact, comparable to some of the WSI values we computed. The variations of the Weather Severity Index among the trajectories, shown in Figure 23, indicate the local quantitative variability of the weather. However, the sequence of scans on each trajectory and the quasi-RHI displays of the radar data in the 2.5-km data window enabled us to determine that the first post-impact scans were adequately representative of the actual reentry weather. One additional point that bears on this problem is that the weather scans were taken not on the actual RV trajectories but on nominal trajectories generated by the KREMS Real-Time Program for the mission. The deviation of the actual trajectory from the nominal is generally not significant from the meteorological point of view. The problems affecting the reliability of the water content and reflectivity values computed from the PMS data have been discussed in detail by Jahnsen et al.[2] and Barnes et al.[4] The most critical factor is the selection of ice crystal habit, which in the present case was fairly certain.

The observational techniques used for the PVM-5 weather data acquisition proved highly effective in terms of pre-mission weather evaluation, rapid access to data for "quick-look" analysis, and correlation of aircraft and radar data. These included the use of the SPA-40 RHI scope at the PRESS Control Center, the computation of water content profiles in near-real-time from the data on the PRESS B-6 tape, and the link-offset mode of obtaining the Z-M correlation data.

References

1. Wilmot, R.A., Cisneros, C.E., and Guiberson, F.L. (1974) High cloud measurements applicable to ballistic missile systems testing, 6th Conf. Aerosp. and Aeronaut. Meteor., Amer. Meteor. Soc., pp 194-199.

2. Jahnsen, L.J., Heymsfield, A.J., and Carbone, R.E. (1974) Final Report of PVM-5 Mission and NEWT WB-57F Instrumentation and Cloud Particle Measurements, MRI 74 FR-1230, Meteorology Research, Inc., Altadena, Calif.

3. Uthe, E.E., Allen, R.J., and Russell, P.B. (1974) Light Detection and Ranging (LIDAR) Support for STM-8W and PVM-5 Reentry Operations, SRI Project 2859, Stanford Research Institute, Menlo Park, Calif.

4. Barnes, A.A., Jr., Metcalf, J.I., and Nelson, L.D. (1974) Aircraft and Radar Weather Data Analysis for PVM-5. AFCRL-TR-74-0627, Air Force Cambridge Research Laboratories, Hanscom AFB, Mass.

5. Metcalf, J.I., Barnes, A.A., Jr., and Kraus, M.J. (1975) Final Report of PVM-4 and PVM-3 Weather Documentation, AFCRL-TR-75-0097, Air Force Cambridge Research Laboratories, Hanscom AFB, Mass.

6. Metcalf, J.I., Barnes, A.A., Jr., and Kraus, M.J. (1975) Final Report of STM-8W Weather Documentation, AFCRL-TR-75-0207, Air Force Cambridge Research Laboratories, Hanscom AFB, Mass.

7. Barnes, A.A., Jr., Nelson, L.D., and Metcalf, J.I. (1974) Weather Documentation at Kwajalein Missile Range, 6th Conf. Aerosp. and Aeronaut. Meteor., Amer. Meteor. Soc., 66-69; AFCRL-TR-74-0430, Air Force Cambridge Research Laboratories, Hanscom AFB, Mass.

8. Metcalf, J.I., Barnes, A.A., Jr., and Nelson, L.D. (1975) Water content and reflectivity measurement by "chirp" radar, 16th Radar Meteor. Conf., Amer. Meteor. Soc., pp 492-495.

9. Trolinger, J.D., Farmer, W.M., and Clayton, F.P. (1974) Development and Application of an Airborne Holography System and Particle Sizing Interferometer, SAI-74-511-TT, Science Applications, Inc., La Jolla, Calif.

10. Heymsfield, A.J. (1973) The Cirrus Uncinus Generating Cell and the Evolution of Cirriform Clouds, PhD Thesis. The University of Chicago.

11. Battan, L.J. (1973) Radar Observation of the Atmosphere, Univ. of Chicago Press, 324 pp.

Appendix A

Derivation and Processing of PRESS B-6 Data

The values of radar cross section used to derive the near-real-time profiles of estimated ice water content were obtained from ALCOR in the following way. From each pulse the four signal values in gates 51, 52, 53, and 54 (centered about the radar tracking point) were examined and the maximum of these four values was stored in a memory unit, which was updated for each successive pulse. Once every 1/10 sec the contents of this memory were transmitted to the PRESS computer, where they were recorded sequentially on the PRESS B-6 tape. In consultation with personnel at PRESS we developed a program to average these values over 1-sec intervals and compute the reflectivity factor Z by Eq. (5). The listing of the 1-sec averaged Z values provided the data for Figures 14, 16, and 18. At the site, these were converted to profiles of ice water content, by means of appropriate Z-M equations, on a hand calculator. Subsequently the PRESS program was modified to compute M by Eq. (7) and WSI by Eq. (3).

We are currently pursuing a detailed evaluation of the effects of the 4-gate "peak selection" scheme, and the number of values averaged, on the resulting Z values. We intend to publish the results in a future report in this series, but some preliminary results are now available. The peak selection process raises the averaged Z values by approximately 2 or 3 dB. (This bias is offset by the 3 dB negative bias in the original value of the constant in Eq. (5) which was written into the PRESS program, so that the B-6 data presented in Section 4 are correct to within about 1 dB.) The peak selection also reduces the fluctuation of the

pulse-to-pulse signal level, so that the averages of 10 samples have standard deviations of less than 2 dB. It should be emphasized that any bias in the computed values of Z does not affect the water content profiles (Figure 22), because the radar data are used as intermediaries between the ice water content computed from the PMS data and the ice water content along the trajectories.

Acronyms and Symbols

AFCRL	Air Force Cambridge Research Laboratories
ALCOR	ARPA-Lincoln C-band Observables Radar
ALTAIR	ARPA Long-Range Tracking and Instrumentation Radar
ARPA	Advanced Research Projects Agency
CDPC	Central Data Processing Computer
DMSP	Defense Meteorological Satellite Program
EG&G	Edgerton, Germeshausen, and Grier, Inc.
ERT	Environmental Research and Technology, Inc.
GMT	Greenwich Mean Time
KMR	Kwajalein Missile Range
KREMS	Kiernan Reentry Measurements Site
LIDAR	Light Detection and Ranging (optical analog of RADAR)
M	Water content (liquid or ice), gm m^{-3}
MRI	Meteorology Research, Inc.
NWS	National Weather Service
PMS	Particle Measuring Systems, Inc.
PPI	Plan Position Indicator
PRESS	Pacific Range Electromagnetic Signature Studies
PVM	Production Verification Missile
RH	Relative Humidity
RHI	Range Height Indicator
ROCC	Range Operations Control Center
RTI	Range Time Intensity

RV	Reentry Vehicle
SAI	Science Applications, Inc.
SAMSO	Space and Missile Systems Organization
SAMTEC	Space and Missile Test Center
SRI	Stanford Research Institute
TRADEX	Target Resolution and Discrimination Experiment
TTR	Target Tracking Radar
WSI	Weather Severity Index
Z	Radar reflectivity factor, $mm^6\ m^{-3}$
Z	Greenwich Mean Time

Printed by
United States Air Force
Hanscom AFB, Mass. 01731